Title

Widespread RNA hypoediting in schizophrenia and its relevance to mitochondrial function

Journal

Science Advances, 9(14)

ISSN

2375-2548

Authors

Choudhury, Mudra
Fu, Ting
Amoah, Kofi
et al.

Publication Date

2023-04-07

DOI

10.1126/sciadv.ade9997

Peer reviewed

HUMAN GENETICS

Widespread RNA hypoediting in schizophrenia and its relevance to mitochondrial function

Mudra Choudhury[1], Ting Fu[2], Kofi Amoah[1], Hyun-Ik Jun[3], Tracey W. Chan[1], Sungwoo Park[3], David W. Walker[3,4], Jae Hoon Bahn[3]*, Xinshu Xiao[1,2,3,4]*

RNA editing, the endogenous modification of nucleic acids, is known to be altered in genes with important neurological function in schizophrenia (SCZ). However, the global profile and molecular functions of disease-associated RNA editing remain unclear. Here, we analyzed RNA editing in postmortem brains of four SCZ cohorts and uncovered a significant and reproducible trend of hypoediting in patients of European descent. We report a set of SCZ-associated editing sites via WGCNA analysis, shared across cohorts. Using massively parallel reporter assays and bioinformatic analyses, we observed that differential 3′ untranslated region (3′UTR) editing sites affecting host gene expression were enriched for mitochondrial processes. Furthermore, we characterized the impact of two recoding sites in the mitofusin 1 (*MFN1*) gene and showed their functional relevance to mitochondrial fusion and cellular apoptosis. Our study reveals a global reduction of editing in SCZ and a compelling link between editing and mitochondrial function in the disease.

INTRODUCTION

RNA editing, the alteration of targeted nucleotides on RNA molecules, notably reshapes our understanding of the central dogma of biology. Most RNA editing sites involve the nucleotide conversion from adenosine to inosine (termed *A*-to-*I* editing) on double-stranded pre-mRNAs catalyzed by the adenosine deaminase (ADAR) enzymes (*1*). As inosines are interpreted as guanosines by the subsequent cellular machineries, *A*-to-*I* editing is synonymously termed *A*-to-*G* editing. An alternative but less prevalent form of editing involves the substitution of cytosine with uracil (*C*-to-*U* or *C*-to-*T* editing), which is conducted by the apolipoprotein B mRNA editing catalytic polypeptide-like (APOBEC) enzymes (*2*). Occurring in both coding and noncoding regions, RNA editing greatly diversifies the transcriptome (*3*). In addition to altering protein sequences, RNA editing may affect many other processes, such as splicing (*4*), RNA stability (*5*), and translation (*6*). Thus, identifying functionally meaningful editing sites can help to understand their primary biological roles and, moreover, elucidate how dysregulated editing contributes to various disorders.

Previous studies of RNA editing have shown the significance of aberrant editing in neurological diseases (*7*). One such disease is schizophrenia (SCZ), in which differences in RNA editing have been profiled in both noncoding and coding regions (*8*). SCZ is a neuropsychiatric disorder characterized by delusional thinking, hallucinations, anxiety, paranoia, and a variety of other psychiatric symptoms (*9*). The disorder is influenced by both genetic and environmental factors, such as stress, substance use, and maternal perinatal infection (*10*). As SCZ is highly heritable, many studies have aimed to identify the genetic basis of the disease and understand the biological pathways implicated in its progression (*10*). Genome wide association studies have identified genetic variants that may collectively influence the disorder (*11*). However, the underlying biological mechanisms involved in shaping the condition beyond genetic mutations are largely unknown. Consequently, investigation of SCZ at the transcriptional and posttranscriptional level has gained traction, as this may yield insights into disease etiology.

Various transcriptomic regions with altered RNA editing have been catalogued in SCZ and many of its related brain disorders. For example, an I/V editing site in the glutamate receptor, ionotropic kainate 2 (*GRIK2*), is known to cause a nonsynonymous change in its protein. GRIK2 modulates cellular Ca^{2+} permeability, and its dysregulation contributes to increased intracellular Ca^{2+} levels observed in patients with bipolar disorder, a mental disease sharing substantial neuropathology with SCZ (*12*, *13*). In addition, global profiling of RNA editing in SCZ has shown dysregulation of hundreds of RNA editing sites, including those in genes involved in translation initiation and α-amino-3-hydroxy-5-methyl-4-isoxazolepropionic acid (AMPA) glutamate and ionotropic receptors (*8*). These studies confirm the importance of editing in this neuropsychiatric disorder and motivate further in-depth investigations on the global profile, regulation, and function of RNA editing in SCZ and related disorders.

In this study, we characterized the RNA editomes in brain samples of patients with SCZ and controls in multiple cohorts from the PsychENCODE consortium via de novo detection of RNA-DNA differences. Comparing data from SCZ and control individuals, we identified 26,841 unique differential editing sites. We observed a significant trend of hypoediting in SCZ, which was reproduced in three of the four cohorts of European individuals. Moreover, our study uncovered close relevance of RNA editing dysregulation to mitochondrial function from two perspectives: RNA editing in 3′ untranslated regions (3′UTRs) of mitochondria-related genes and the impact of two recoding editing sites in the mitofusin 1 (MFN1) protein. Together, our study delineates a comprehensive landscape of RNA editing in SCZ, reports a replicable hypoediting bias in SCZ, and reveals functional relevance of RNA editing in mitochondria-related processes.

[1]Bioinformatics Interdepartmental Program, University of California, Los Angeles, CA, USA. [2]Molecular, Cellular, and Integrative Physiology Interdepartmental Program, University of California, Los Angeles, CA, USA. [3]Department of Integrative Biology and Physiology, University of California, Los Angeles, CA, USA. [4]Molecular Biology Institute, University of California, Los Angeles, CA, USA.
*Corresponding author. Email: gxxiao@ucla.edu (X.X.); jbahn@ucla.edu (J.H.B.)

RESULTS

RNA editing sites detected in patients with SCZ and controls of the BrainGVEX data

We first aimed to identify global RNA editing profiles in SCZ to further understand functional pathways dysregulated in the disease. We obtained brain frontal cortex (FC) RNA sequencing (RNA-seq) data of 170 samples from the BrainGVEX cohort in the PsychENCODE consortium (table S1) (*14*). The RNA-seq libraries were generated using ribosomal RNA depleted total RNA (*14*). On average, 41 million reads were uniquely mapped per sample (fig. S1A). Following sequence alignment and quality control procedures, 65 SCZ and 67 control samples were retained (Materials and Methods), the vast majority (96%) being from European populations. We ensured that metadata variables and data-related metrics [e.g., age, gender, RNA integrity number (RIN), postmortem interval (PMI), and sequencing depth] did not significantly differ between SCZ and control individuals (fig. S2, A and B).

RNA editing sites were detected using our previously developed de novo RNA editing detection pipeline (*15*–*17*). As editing sites are often close to one another within a region of the transcriptome, we further implemented a method to detect sites within these "hotspots" that may be otherwise missed by conventional mapping software (*18*, *19*) (Materials and Methods). In total, we detected 4,576,706 RNA editing sites in the FC of the BrainGVEX cohort. To avoid sites with rare occurrences, we discarded those with nonzero editing in less than 10% of the samples. Following this filter, a total of 255,812 sites were retained, referred to as "common" RNA editing sites (Fig. 1A). Of all *A*-to-*G* common sites, 212,472 (85%) overlapped with known RNA editing sites cataloged in the REDIportal database (fig. S1B) (*20*).

On average, we observed that greater than 98% of all common editing sites, and the majority of loci in nonrepetitive and coding regions, were *A*-to-*G* loci in each sample, demonstrating the high accuracy of the de novo detection pipeline (Fig. 1B and fig. S1, C and D). It is well known that RNA editing identification in nonrepetitive or coding regions is challenging (*17*). As shown in fig. S1D, we achieved a high percentage of *A*-to-*G* in nonrepetitive regions but relatively lower percentage in the coding regions, as expected. Given the overall high *A*-to-*G* percentage, we included all predicted RNA-DNA differences in the analyses hereafter, unless otherwise noted. Consistent with previous studies (*17*), the majority of editing sites resided in Alu elements (fig. S1E) and intronic regions (fig. S1F). As expected, the number of sites detected per sample correlated approximately with the total read coverage of each sample (fig. S1G). We calculated common site RNA editing average (CREA) per sample using all common sites with at least five reads. An Alu-specific CREA was also calculated using common sites in Alu regions. Both CREA and Alu-CREA had significantly positive correlations with *ADAR2* expression and negative correlations with *ADAR3* expression, while both insignificantly correlated with the expression of *ADAR1* (fig. S1H).

Differential editing analysis in BrainGVEX data and reduced editing in Europeans with SCZ

Using our previous methods (*19*), we detected 13,997 differential editing sites between SCZ and controls in the BrainGVEX cohort (Fig. 1A and Materials and Methods). To represent overall editing level of these differential editing sites per sample, we calculated the average editing ratio of all differential sites with ≥5 reads in each sample, hereby referred to as the differential site RNA editing average (DREA). In comparing SCZ and control samples, we observed significantly lower DREA values in the SCZ samples (Fig. 1C). The SCZ and control samples were clearly segregated when clustered based on the differential editing sites, which validates the nature of differential editing (Fig. 1D). In addition, differential sites that were hypoedited in SCZ greatly outnumbered those that have increased editing in the disease (Fig. 1E). Gene ontology (GO) analysis revealed that differential editing sites occurred in genes involved in various brain-related pathways such as motor neuron axon guidance, synaptic transmission, and ion transport (fig. S1I).

Among the differential editing sites, a number of them cause nonsynonymous amino acid changes, stop loss, or stop gain (recoding sites) (Fig. 1F). Some of these sites are known to have relevance in neuropsychiatric diseases. One example is the aforementioned I/V recoding site in *GRIK2*, a gene encoding the well-known ionotropic glutamate receptor implicated in mood disorders. In SCZ, we observed hypoediting of this site (Fig. 1F), which is similar to that reported in bipolar disorders (*12*). This hypoediting event can lead to an increase in intracellular Ca^{2+} levels (*12*). Furthermore, we observed significantly decreased editing for sites that have not been studied previously in SCZ, such as a *C*-to-*T* site in the mitochondrial fusion gene *MFN1* (Fig. 1F), which is further examined below.

Investigation of differential loci and expression of differentially edited genes in single-nucleus RNA-seq

As RNA editing may be highly cell type specific (*21*), we next asked whether the differential editing patterns in SCZ may have originated from specific cell types. To address this question, we analyzed single-nucleus RNA-seq data from prefrontal cortex (PFC) of control samples in a previous study (*22*). Six major brain cell types, excitatory and inhibitory neurons, astrocytes, oligodendrocytes, microglia, endothelial, and oligodendrocyte progenitor cells (OPCs), were obtained from 24 samples. We examined gene expression and editing profiles of each cell type (by pooling cells of the same type). Excitatory and inhibitory neurons expressed the highest fraction of genes that were differentially edited in the bulk brain tissue of SCZ, followed by oligodendrocytes, astrocytes, and OPCs (Fig. 1G). Next, we asked whether the differentially edited sites in the bulk brain of SCZ were edited in each cell type. Among all observed editing sites in each cell type, the fraction of sites that were differentially edited in the bulk data is highest in neurons (Fig. 1H). These observations suggest that differential RNA editing observed in the bulk RNA-seq analysis may reflect editing differences in neurons to a larger extent than in other cell types.

Given the above RNA editing differences among cell types, we next asked whether cell type proportions were different between the bulk SCZ and control samples, which may contribute to the observed differential editing profiles. We used the CIBERSORTx software (*23*) to calculate the relative proportion for five cell types of brain FC—neurons, oligodendrocytes, microglia, endothelial cells, and astrocytes—using gene expression of known cell type signature genes (*24*). We observed an insignificant difference in cell type proportion between SCZ and control samples (fig. S1J). Thus, the differential editing observed between the two groups may not have

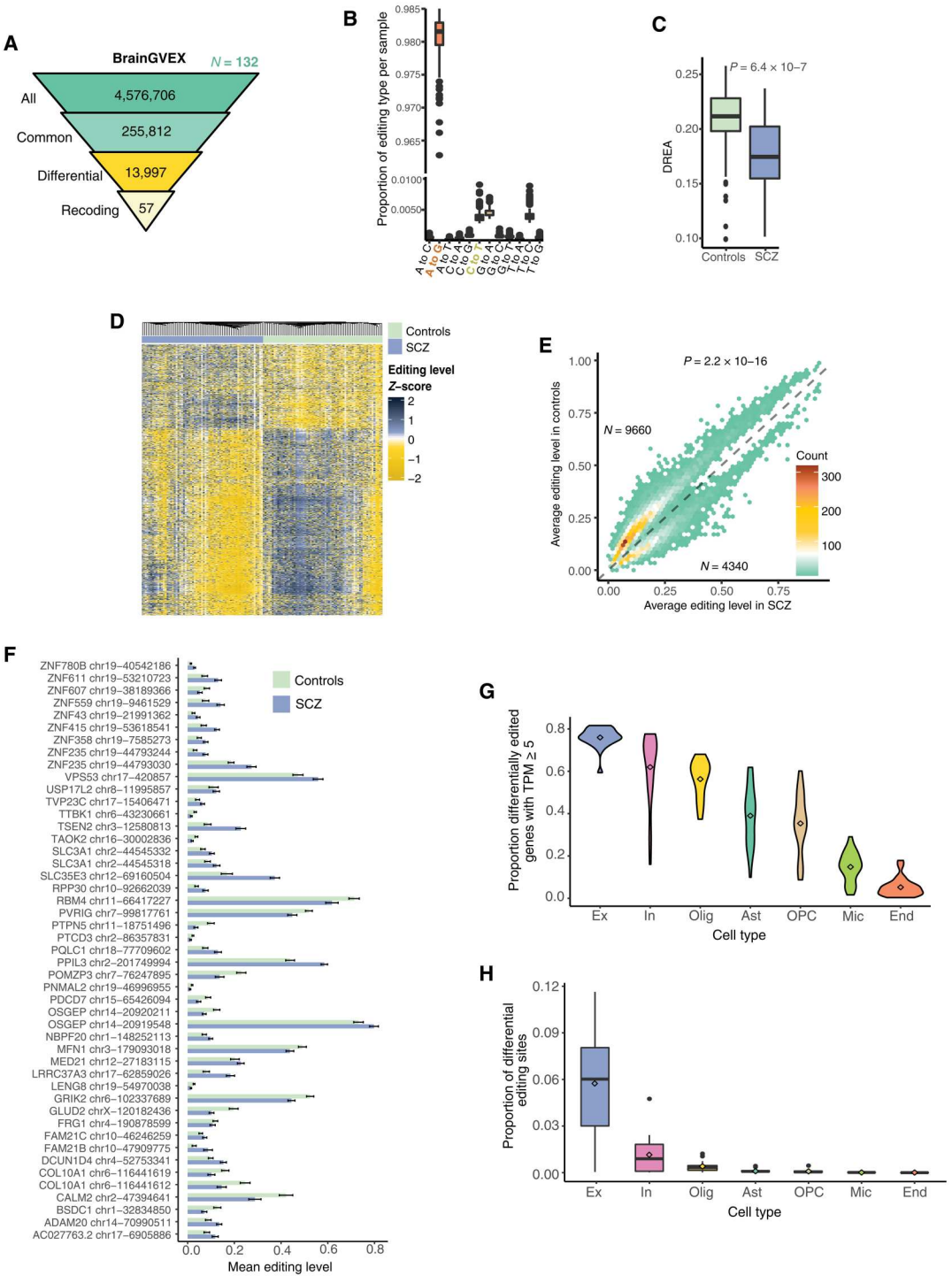

Fig. 1. Overview of RNA editing analysis in the BrainGVEX cohort. (**A**) Summary of editing sites detected in each step of the RNA editing analysis. Top to bottom: All detected RNA-DNA differences (RDDs), common sites with nonzero editing in ≥10% of samples, sites differentially edited between SCZ and control (see Materials and Methods), and nonsynonymous protein recoding sites among the differential sites. *N* = 132, total number of samples included in the analysis. (**B**) Proportion of each type of RDD among common sites detected per sample. (**C**) DREA per sample separated by condition for all differential sites covered by least five total reads. *P* value was calculated via Wilcoxon rank sum test. (**D**) Hierarchical clustering of differential editing sites (rows) and samples (columns). *Z*-scores were calculated for each site across all samples. (**E**) Average editing levels of differential editing sites in SCZ and controls. Numbers (*N*) of editing sites that were up- or down-regulated in SCZ are shown, which were compared via chi-square test (*P* value shown at the top). (**F**) Editing levels in controls or SCZ of each differential protein recoding site. Error bars correspond to the SEM. (**G**) Proportion of genes with ≥5 TPM in each cell type among all differentially edited genes in the single-nucleus RNA-seq data. Ex, excitatory neurons; In, inhibitory neurons; Olig, oligodendrocytes; Ast, astrocytes; OPC, oligodendrocyte progenitor cells; Mic, microglia; End, endothelial cells. (**H**) Proportion of observed editing sites in each cell type among all differentially edited sites. Cell type abbreviations are the same as in (G).

arisen from cell type proportion differences. In contrast, using differential editing sites located in the signature genes of each cell type, we observed that the mean DREA was reduced in SCZ for the majority of cell types (fig. S1K). These observations further support the global hypoediting trend observed in the bulk data of SCZ.

Differential RNA editing analysis in additional cohorts

To validate global editing patterns discovered in the BrainGVEX cohort, we identified RNA editing sites in an additional cohort in the PsychENCODE database, referred to as the CommonMind Consortium (CMC) (table S1) (*25*). The same analysis methods used for the BrainGVEX data were adopted here. While the CMC cohort had a larger number of samples than the BrainGVEX cohort, close to half of the CMC subjects were above the age of 70 years old

(an age group not present in the BrainGVEX cohort; fig. S2A). In addition, samples in the 70+ age group showed significantly lower quality (indicated by RIN) than the <70 age group. These samples from older individuals yielded RNA-seq data with a lower proportion of mapped mRNA bases and a higher proportion of intergenic bases (fig. S3, A to C). Considering the possibility of lower data quality from samples with 70+ age and focusing on the goal of validating the global editing patterns of BrainGVEX, we only used CMC samples from subjects below 70 years of age. After quality control procedures and meta-data matching (Materials and Methods), 137 samples (79% European) were retained for RNA editing analysis and differential editing detection (fig. S4, A and B). The total number of detected sites, common sites (edited in ≥10% of samples), differentially edited sites, and recoding sites are shown in Fig. 2A. Using the differential editing sites, we calculated the DREA for each sample and observed a significant trend of reduced editing in SCZ (Fig. 2A), consistent with the observation in the BrainGVEX cohort.

Next, we analyzed data from two additional PsychENCODE cohorts, the CMC Human Brain Collection Core (HBCC) and the Lieber Institute for Brain Development (LIBD). Since these two cohorts included samples from European origin along with a sizeable number of samples of African American descent, we analyzed data from the two ethnicities separately. After quality control procedures, we analyzed 18 SCZ, 23 controls, and 17 SCZ, 20 controls of European-descent from HBCC and LIBD, respectively. Despite the relatively small sample size, we observed a significant hypoediting trend in SCZ of the HBCC cohort (Fig. 2B). No significant difference was detected in the LIBD data (Fig. 2C). Thus, RNA editing levels were significantly reduced in SCZ in three of the four European-dominant cohorts.

In addition, we analyzed data from 48 SCZ, 52 controls (HBCC) and 18 SCZ, 26 controls (LIBD) of African American-descent. Opposite to the reduced editing in SCZ observed in European samples, a significant increase in DREA of SCZ relative to controls was detected in both cohorts (fig. S5A). Using CIBERSORTx, we did not observe a significant difference in cell type proportion between SCZ and controls (fig. S5B). While the DREA of signature genes of each cell type was higher in SCZ than controls for most cell types in both cohorts, it only reached significance in astrocytes (HBCC) and oligodendrocytes (LIBD) (fig. S5C). Thus, we hypothesize that the hyperediting trend in SCZ of African American individuals may be due to ethnicity-related differences in RNA editing, a topic that needs to be further investigated.

WGCNA of edited loci and detection of robust modules of editing sites associated with SCZ

We next examined whether differential editing sites were shared between the BrainGVEX and CMC data (the HBCC and LIBD cohorts were not included due to their relatively small numbers of European subjects). While 314 overlapping differentially edited sites were observed between the cohorts, the total overlap did not reach statistical significance (fig. S6A). However, genes harboring differential editing sites showed a significant overlap, suggesting a similarity in functional pathways being differentially edited (fig. S6B).

To further evaluate SCZ-relevant editing sites shared between the two cohorts, we carried out the weighted gene coexpression network analysis (WGCNA) (*26*) on common RNA editing sites (Materials and Methods) in each cohort. The goal of this analysis was to identify RNA editing modules (i.e., sites with correlated editing levels across samples) that are associated with disease condition. For each cohort, WGCNA yielded multiple modules (fig. S7, A and B), the eigengenes of which were then correlated with the disease condition while considering confounding meta-data covariates (age, gender, RIN, etc.; see Materials and Methods). We observed that the largest module—labeled as the "turquoise" module—significantly correlated with SCZ in BrainGVEX and CMC, respectively (fig. S7C). Editing sites in turquoise modules of the two cohorts significantly overlapped with each other when considering editing sites testable in both cohorts (Materials and Methods, Fig. 2D, and table S2).

The two cohorts also shared a significant number of genes harboring turquoise module editing sites, as expected (Fig. 2E). GO analysis of the shared genes uncovered many pathways related to brain functionality and neuronal signaling, such as ionotropic glutamate receptor activity and synapse assembly (Fig. 2F). One of the top GO terms identified is related to mitochondrial fragmentation in apoptotic process (Fig. 2F), consistent with previous literature that implicated mitochondrial dysregulation as an important aspect of SCZ (*27*) (Discussion). Together, these data support the existence of reproducible differential editing profiles in SCZ, many located in genes with functional relevance to brain function.

Enrichment of potentially functional 3′UTR editing sites in mitochondria-related pathways

Given the large number of differential editing sites in SCZ, it is important to investigate their functional relevance. To this end, we first focused on sites in the 3′UTRs given the observed relative enrichment of differential sites in this region (fig. S6C). Since 3′UTRs are enriched with cis-regulatory elements, RNA editing in the 3′UTRs may affect posttranscriptional gene regulation, for example, mRNA abundance, as shown in previous studies (*5*, *28*). To experimentally screen for functional 3′UTR editing sites in regulating mRNA abundance, we performed a massively parallel reporter assay (MPRA), similar to those adopted to discover functional 3′UTR single-nucleotide polymorphisms (Fig. 3A and Materials and Methods) (*29*). Although the edited version of the RNA editing site was hard-coded into the DNA of the reporters, this design represents a reasonable approximation to assay for the impact of a 3′UTR editing site on mRNA abundance. This is because such regulation most likely occurs in the cytoplasm, independent of the process of RNA editing.

In the MPRA, we included a total of 770 differential *A*-to-*G* editing sites located in 3′UTRs, consisting of all differential 3′UTR *A*-to-*G* sites detected in the BrainGVEX and CMC cohorts, and a small number from the HBCC or LIBD data. Comparing the relative enrichment of the unedited and edited versions of a site in the plasmid DNA input and expressed mRNA, we identified 214 editing sites (28% of 770 testable sites, located in 160 genes; table S3) that resulted in significant reporter expression changes [false discovery rate (FDR) ≤ 0.1 and |ln(Fold Change)| ≥ 0.1; Fig. 3B and Materials and Methods]. Thus, a relatively large fraction of 3′UTR editing sites may regulate gene expression posttranscriptionally. The GO analysis of genes harboring significant sites identified in the MPRA revealed a number of pathways related to mitochondrial function or translational regulation (Fig. 3C).

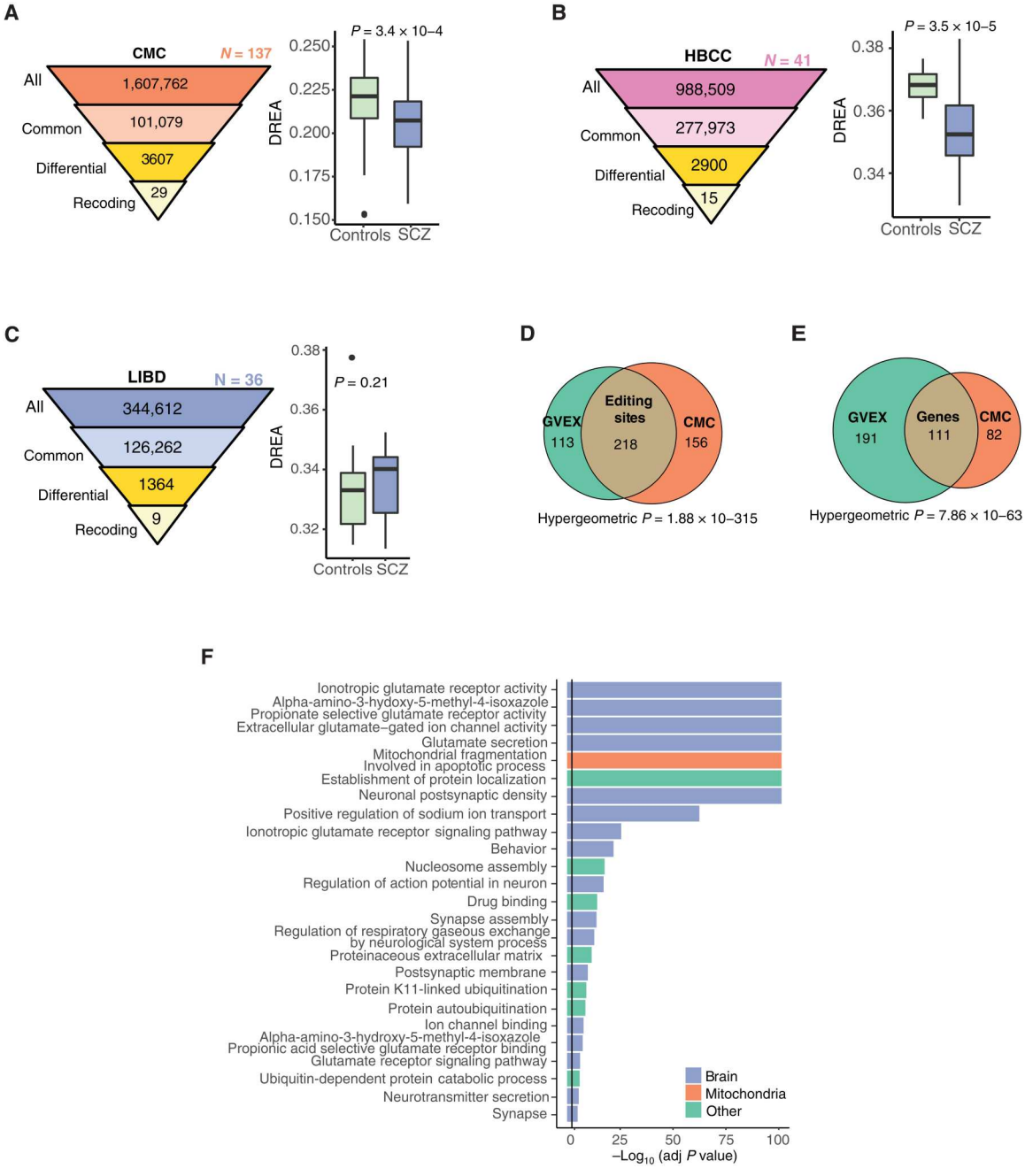

Fig. 2. Comparison of RNA editing across cohorts. (**A** to **C**) Summary of editing sites detected in each step of the RNA editing analysis for the CMC, HBCC, and LIBD cohort, respectively, similar to Fig. 1 (A and C). (**D**) Overlap between RNA editing sites in the turquoise modules resulting from WGCNA of the BrainGVEX and CMC cohorts. Only sites testable for both cohorts are displayed. *P* value was determined via the hypergeometric test. (**E**) Similar to (D) but for genes harboring editing sites in the turquoise modules. (**F**) GO enrichment analysis of genes shared by the BrainGVEX and CMC analysis in (E).

As a complementary approach, we examined the correlation between the editing levels of 3′UTR differential editing sites (tested in the MPRA) and the expression levels of their host genes in the respective cohorts (Fig. 3D). We found that 74 of 741 bioinformatically testable editing sites were significantly correlated with gene expression (Materials and Methods). These sites were located in 65 genes, 30 of which overlapped with the genes with significant MPRA results ($P = 1.7 \times 10^{-46}$, hypergeometric test). Consistent with the MPRA results, genes containing the 74 sites were significantly enriched with mitochondria-related pathways, such as respiratory electron transport chain, mitochondrial inner membrane, and mitochondrial matrix (Fig. 3C).

To further examine the potential function of genes whose 3′UTR editing was associated with gene expression (3′UTR EdEx genes), we analyzed functional pathways enriched among the union of 195 such genes discovered experimentally or bioinformatically.

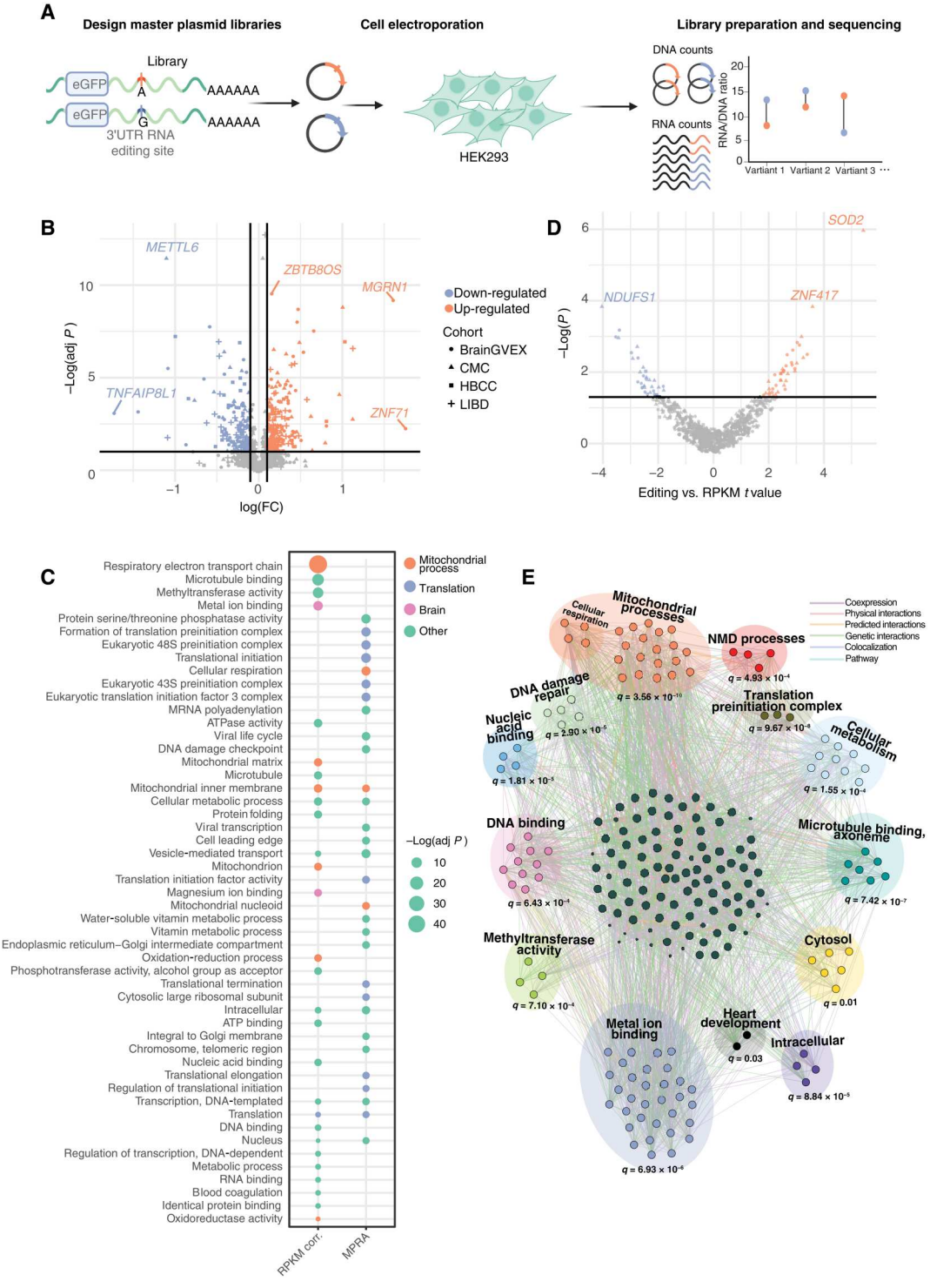

Fig. 3. 3′UTR editing associated with gene expression. (**A**) Schema of the MPRA experiment to identify functional 3′UTR *A*-to-*G* editing sites that alter gene expression. (**B**) Expression fold change and adjusted *P* value (see Materials and Methods) of 3′UTR editing sites included in the MPRA. Purple and orange dots correspond to editing sites that significantly alter gene expression [FDR ≤ 0.1 and |ln(Fold Change)| ≥ 0.1]. (**C**) GO enrichment analysis of genes containing 3′UTR differential editing sites associated with gene expression through experimental (MPRA) or bioinformatic (RPKM correlation) analysis. ATPase, adenosine triphosphatase. (**D**) Significance (*P* value) and directionality (*t*-statistic, jittered for visualization) of the correlation between editing levels of 3′UTR *A*-to-*G* differential editing sites and their respective gene expression levels. Orange and purple colors denote $P < 0.05$. (**E**) Gene network constructed by GeneMANIA (*30*) for the union of significant genes in (B) and (D). Genes are grouped into biological categories based on GO enrichment analysis. The most significant *q* value for the overarching GO category is displayed.

Via the GeneMANIA database (*30*) and Cytoscape visualization tool (*31*), we created a network of previously curated associations between the 195 3′UTR EdEx genes, as well as 20 additional highly related genes predicted by GeneMANIA (Materials and Methods). We observed that the 3′UTR EdEx genes are highly interconnected, largely through genetic interactions (Fig. 3E). Among all modules of the network, mitochondrial processes harbored the most genes with the most significant enrichment level (Fig. 3E). Together, these analyses support that differential editing in the 3′UTR may affect mitochondria-related genes by altering their gene expression in SCZ.

RNA editing of *MFN1* leading to reduced mitochondrial fusion

In addition to editing sites in nonprotein coding regions, many of the protein recoding sites identified as differential in SCZ have interesting and diverse functionalities. As examples, we focused on two recoding sites in the gene *MFN1* that encodes a mitochondrial membrane protein essential for mitochondrial fusion (*32*). One of the sites included a *C*-to-*T* recoding event in *MFN1* with differentially reduced editing levels in SCZ (Fig. 4A). Another *A*-to-*G* editing site is located in the adjacent codon to the *C*-to-*T* site, which was not differentially edited in SCZ. We confirmed the presence of both RNA editing sites in human brain samples (Fig. 4B). Further investigation revealed that both editing sites detected in our analyses are conserved across species such as *Macaca mulatta* (*33*), mouse (*34*), and zebrafish (*35*) (fig. S8A). In addition, we observed that the editing levels of the *MFN1 C*-to-*T* and *A*-to-*G* loci are correlated with each other, as editing of the *A*-to-*G* site is more likely if the *C*-to-*T* editing is present (fig. S8B). In mouse N2a cells, we confirmed that the *C*-to-*T* editing site is regulated by Apobec2 (Fig. 4C and fig. S8C), a known *C*-to-*T* editing enzyme in mouse (*36*), further supporting the validity of this edited locus.

Next, we examined the impact of the two editing sites on mitochondrial fusion, a well-established function of MFN1 (*37*). We first used mouse embryonic fibroblast (MEF) cells with *Mfn1* and *Mfn2* double knockout (dKO). Overexpression vectors of *Mfn1* and its edited versions (I328V from *A*-to-*G* editing, S329L from *C*-to-*T* editing, and I328V + S329L double editing) were generated and introduced into dKO MEF cells. Expression of the Mfn1 proteins were confirmed via Western blot (Fig. 4D). The mitochondria morphology was examined via mitoTracker (Fig. 4E). Consistent with previous literature (*37*), we observed a severe fragmented mitochondria phenotype in Mfn1/2 dKO cells (Fig. 4E). In contrast, rescuing by the wild-type (WT) Mfn1 in the dKO background showed 48% long tubular mitochondria, indicating that Mfn1 overexpression restored mitochondrial fusion. Expression of single-edited Mfn1 mutant (I328V or S329L) led to moderate mitochondria morphologies encompassing fragmented, short, and long tubular phenotypes. Notably, the double-edited mutant (I328V + S329) induced significantly less long tubular (16%) and more short tubular (49%) mitochondrial phenotypes (Fig. 4E). Thus, our data suggest that the two recoding sites in Mfn1 reduced the protein′s function in mitochondrial fusion.

As an alternative strategy, we created mutant HEK293T cells that carried the edited bases in their genome by prime editing (*38*). Specifically, cells with a single mutation (corresponding to the I328V or S329L site) or double mutations (I328V + S329L) were generated. Clones with heterozygous mutations were retained (fig. S8D). We confirmed that there was no change in MFN1 and MFN2 expression between WT and mutant cells (fig. S8E). Note that WT human embryonic kidney (HEK) 293T cells do not exhibit RNA editing in either editing site. In WT HEK293T cells, we observed 63% long tubular and 14% fragmented mitochondria (Fig. 4F). In contrast, the double-mutant cells had a significantly higher fraction of fragmented (51%) and lower fraction of long tubular (5%) mitochondria, whereas the single-mutant cells demonstrated intermediate phenotypes between the WT and double-mutant cells (Fig. 4F). Thus, the edited versions of MFN1 induced significant reduction of mitochondrial fusion. This observation is largely consistent with that observed in mouse cells, despite the differences in the two systems (e.g., the presence of endogenous MFN2 in HEK293T cells versus the absence of MFN2 in MEF cells).

To further investigate the impact of *MFN1* editing on mitochondrial fusion, we performed a stress-induced mitochondrial hyperfusion test (*39*). We treated HEK293T cells with cycloheximide, a widely used inhibitor for translational elongation, as a stress to induce mitochondrial hyperfusion, similarly as in previous studies (*40*). We observed that 52% of WT cells had hyperfused mitochondria, whereas only 16% of double-mutant cells underwent hyperfusion (Fig. 4G). Thus, cells with double-edited MFN1 had impaired hyperfusion response given cycloheximide, indicating a possible defect in adaptive stress response of these cells.

RNA editing of *MFN1* and cellular apoptosis

Mitochondria are central players in cell apoptosis. It is known that mitochondrial fission and fusion processes are closely implicated in apoptosis, and loss of MFN1/2 leads to increased apoptotic sensitivity (*41*). Thus, we evaluated the potential impact of RNA editing of *MFN1* on apoptosis. To this end, we measured the level of cytochrome C (Cyt C) in the cytoplasmic and mitochondrial fractions of the above WT and mutant HEK293T cells. Release of Cyt C from the mitochondria into the cytosol is a known hallmark of apoptosis (*42*). As expected, in the WT (untreated) cells, Cyt C was primarily localized in the mitochondrial fraction. In contrast, mutant cells with edited versions of MFN1 showed increased Cyt C in the cytosol, with the double edited cells showing the highest levels of Cyt C release (Fig. 5A).

To corroborate the above observations, we measured the level of cell death via propidium iodide (PI) staining. As shown in Fig. 5B, very few apoptotic cells were detected in the WT cells, as expected. In contrast, the mutant cells carrying one or both edits showed a significantly higher level of apoptosis, with the double edited cells being the highest. This observation is consistent with the results obtained via the Cyt C release assay. Thus, both experiments suggest that the RNA editing sites in *MFN1* affect cellular apoptosis.

DISCUSSION

Our study yields the most comprehensive investigation of dysregulated RNA editing in SCZ to date. We uncovered a common trend of hypoediting in individuals with SCZ across multiple cohorts of primarily European-descent. Furthermore, we investigated the possible functional consequences of differential editing sites in 3′UTRs using MPRA. This experiment, complemented by bioinformatic analysis, revealed hundreds of 3′UTR editing sites that may alter mRNA expression. Many of these functional editing sites are located in genes with relevance to mitochondria function. We

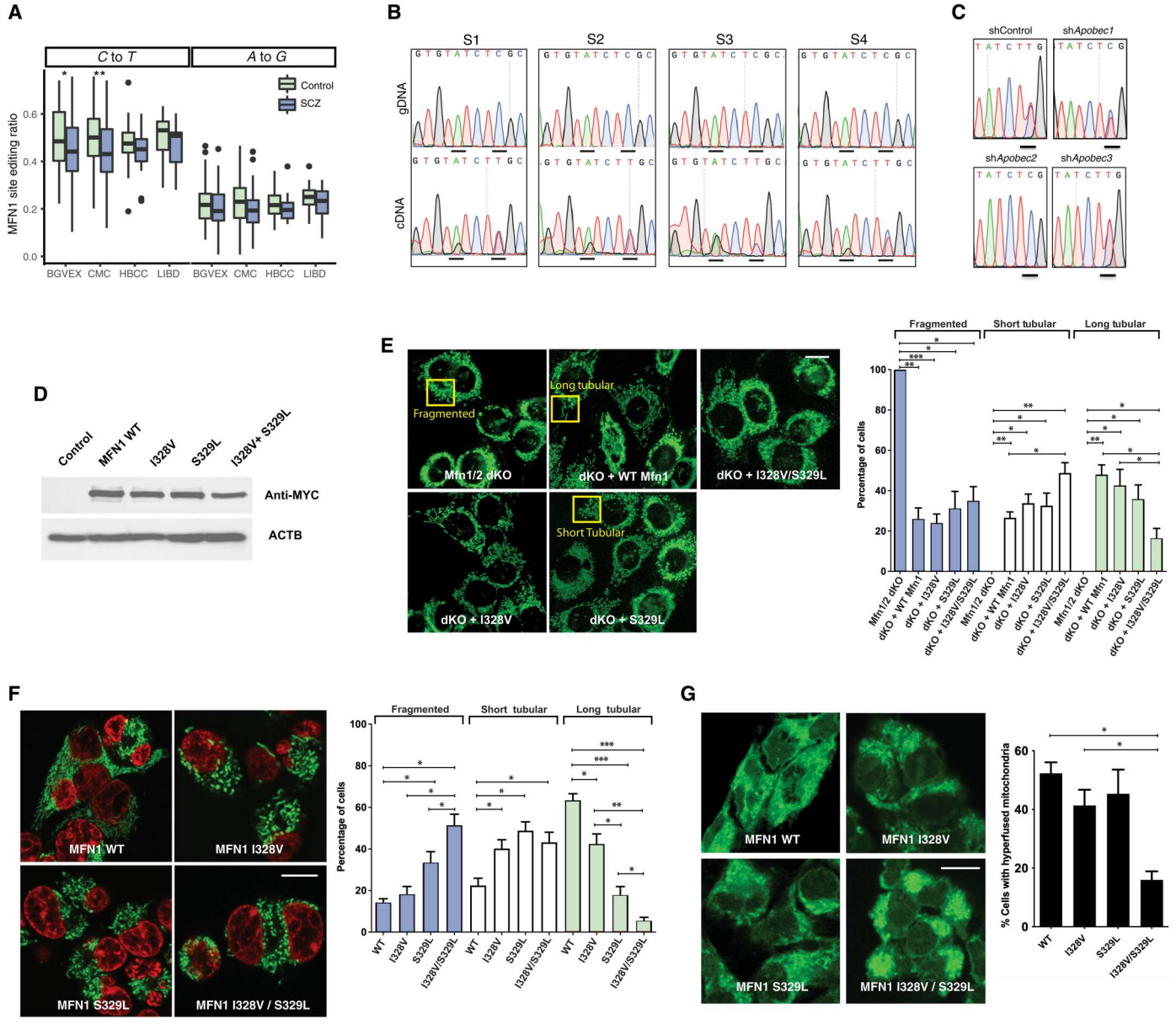

Fig. 4. Functional characterization of MFN1 editing in mouse and human. (**A**) *MFN1 C*-to-*T* and *A*-to-*G* editing levels per cohort for SCZ and Control samples. **P* < 0.05 and ***P* < 0.001, Wilcoxon rank sum test. (**B**) Experimental validation of the *C*-to-*T* and *A*-to-*G MFN1* RNA editing sites in four human brain samples (S1 to S4). Sanger sequencing traces of genomic DNA (top) and cDNA (bottom) are shown, with the *A*-to-*G* (left) and *C*-to-*T* (right) editing sites underlined. (**C**) Experimental testing of the *C*-to-*T* editing site (underlined) in mouse N2a cells with control shRNA (shControl) or shRNA targeting *Apobec1*, *Apobec2*, or *Apobec3*, respectively. Sanger sequencing traces of cDNAs are shown. (**D**) Stable expression of wildtype (WT) Mfn1 and editing mutants (Mfn1 I328V, S329L, and I328V/S329L) (with Myc tags) in Mfn1/2 dKO MEF cells measured by Western blot. Control: empty vector expression. (**E**) Mitochondrial morphology in Mfn1/2 dKO MEF cells with stable expression of WT and mutant Mfn1/2 as shown in (D). Mitochondria was stained by 100 nM MitoTracker (green) for 30 min. Scale bar, 10 μm. Bar plots show quantification of mitochondrial morphology of 120 cells in three biological replicates (**P* < 0.05, ***P* < 0.001, and ****P* < 0.0001, unpaired two-tailed *t* test). Error bars: ±SEM. (**F**) Mitochondrial morphology in HEK293T cells with WT MFN1 or MFN1 editing mutants (MFN1 I328V, S329L, and I328V/S329L). Green, MitoTracker staining for mitochondria; red, Hoechst staining for nucleus. Scale bar, 10 μm. Bar plots show quantification of mitochondrial morphology of 100 cells in three biological replicates. (**P* < 0.05, ***P* < 0.001, and ****P* < 0.0001, unpaired two-tailed *t* test). Error bars: ±SEM. (**G**) Mitochondrial morphology of WT and mutant HEK293T cells treated with cycloheximide for 30 min. Mitochondria were stained by MitoTracker (green). Scale bar, 10 μm. Bar plots indicate cell counts with hyperfused mitochondria (**P* < 0.05, unpaired two-tailed *t* test). Error bars: ±SEM.

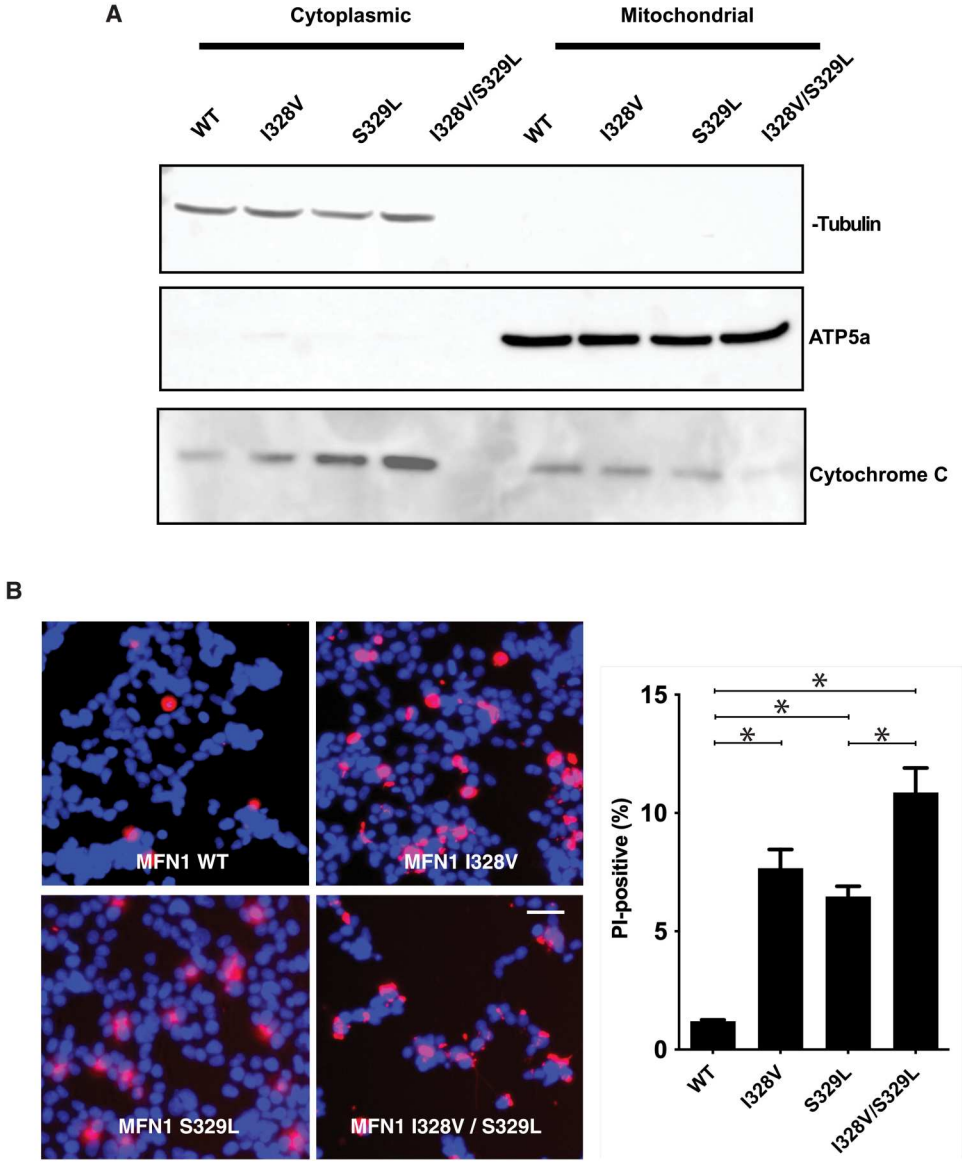

Fig. 5. The effect of MFN1 editing on Cyt C release and cell death. (**A**) Western blot of Cyt C, β-tubulin (cytoplasmic marker), and ATP5a (mitochondrial marker) in mitochondrial and cytoplasmic fractions of HEK293T cells (WT and MFN1 mutants). (**B**) PI staining of HEK293T cells (WT and MFN1 mutants) to measure cell death. Scale bar, 10 μm. Bar plots show % of dead cells (*P < 0.05, unpaired two-tailed t test). Error bars correspond to ±SEM.

also uncovered the functions of two recoding editing sites in *MFN1*, an important gene for mitochondrial fusion.

Previous studies of neurological and neuropsychiatric disorders demonstrated the relevance of RNA editing to brain functionality. For example, our group's work on autism spectrum disorders (ASD) revealed RNA editing changes in genes involved in glutamate receptor activity and synaptic transmission (*19*), which are analogous to those uncovered in this study. A significant hypoediting trend was observed in ASD. Other studies also identified reduced editing in brain disease for specific sites, such as those in the glutamate receptor GRIK2 in bipolar disorder (*12*) and the AMPA/kainate receptor GluR2 in amyotrophic lateral sclerosis (*43*). These studies highlight the significance of reduced editing in the dysregulation of brain function.

The global reduction of RNA editing in the EU SCZ cohort not only implies deregulation of a myriad of biological processes but also alludes to disrupted mechanisms of editing. For example, reduced RNA editing has been shown to elicit immune response via increased ADAR3 expression, a known RNA editing repressor (*44*). Our findings support the association between ADAR3 and reduction of editing, as reflected in the significant negative correlation between overall editing levels and *ADAR3* gene expression (fig. S1H). In addition, we observed a significant positive correlation between editing and *ADAR2* gene expression (fig. S1H). We speculate that hypo-editing in SCZ may have resulted from a combined regulatory impact of ADAR2 and ADAR3 (with a possible involvement of other proteins). ADAR1 may not be a main driver of the hypoediting pattern, given the insignificant correlation (fig. S1H).

Future work is required to further investigate the regulatory mechanisms of hypoediting in SCZ.

A recent global analysis of RNA editing in SCZ did not observe this distinct hypoediting trend for their reported differential sites, although reduced editing in AMPA-type glutamate receptors and postsynaptic density proteins was observed (*8*). A number of factors may have contributed to the distinction between ours and the previous study. We implemented strict quality control procedures, focused on a consistent age range for all cohorts (<70 years), and carried out a rigorous de novo detection of RNA editing sites that allowed us to identify a large number of loci. Furthermore, the European and African American cohorts showed opposite overall trend of editing changes in SCZ, which were not analyzed separately in the previous study (*8*).

In contrast to the hypoediting trend in SCZ of the European cohorts, the African American cohorts showed an overall hyperediting bias in SCZ. Our analysis suggests that the hyperediting trend in African American samples exists in multiple cell types, as shown when only cell type–specific marker genes were analyzed. These results suggest the possible existence of mechanistic differences in RNA editing regulation in SCZ between diverse ancestral populations, an aspect that needs to be investigated in the future. Investigation of most neurological and neuropsychiatric disorders has thus far been conducted largely in European ancestries. Lack of knowledge of disease etiology spanning various ancestries may yield consequential disparities in patient diagnosis and treatment. Our findings highlight the significance of broad ancestry representation in disease studies.

We observed that differential editing sites were enriched in genes functionally important to the brain and mitochondria. Through GO enrichment of differentially edited loci in SCZ, we revealed mitochondrial fragmentation involved in apoptotic processes as a top biological term (Fig. 2F). For EdEx genes detected via MPRA and bioinformatic analyses, an enrichment for mitochondrial processes was again observed. Furthermore, we identified two recoding sites in the mitochondrial fission and fusion protein, MFN1, whose editing was associated with cell survival (Fig. 5B). Mitochondrial dysregulation has been implicated in SCZ by many studies (*27*). Disruption in gene networks related to mitochondrial processes may lead to dendritic spine deficits and onset of SCZ symptoms (*45*). In addition, abnormal SCZ brain connectivity may be associated with aberrant mitochondrial dynamics (*27*). Last, a reduced number of mitochondria was observed in certain layers of the neuronal somata and axospinous synapse terminals of SCZ brains (*46*). Our findings further bolster the important implications of mitochondrial function in SCZ by demonstrating the alteration of expression or function of mitochondria-related genes by RNA editing.

We highlighted the function of two RNA editing sites located in the *MFN1* gene, one of which is hypo-edited in SCZ. Using both mouse and human cells, we observed that the RNA editing recoding sites affect MFN1 function in mitochondrial fusion and cellular apoptosis. Previous work has shown that the ablation of MFN1 in mice leads to midgestational death, for which the embryonic fibroblasts display fragmented mitochondria due to significant reduction in mitochondrial fusion (*37*). MFN1-mediated mitochondrial fragmentation has been suggested to lead to neurotoxicity in induced pluripotent stem cells (*47*). In addition, low expression of MFN1 can lead to neuropathy, such as Charcot-Marie-Tooth disease, a neurodegenerative disease characterized by the demyelination of peripheral nerves (*48*). To our knowledge, the literature on the potential impact of RNA editing on mitochondrial function is very limited. For example, *C*-to-*U* editing by the APOBEC3G protein was predicted to suppress mitochondrial respiration relative to glycolysis in HuT78 cells (*49*). However, the specific editing sites involved in such functions remain unknown. Thus, our study fills a substantial gap by connecting RNA editing to important mitochondrial processes.

Mitochondria are highly dynamic, and a balance between mitochondrial fusion and fission is important to brain development and function (*50*). While the role of MFN1 is to regulate mitochondrial morphology, the relationship between mitochondrial morphology and a healthy homeostasis is complex. Healthy cells require a delicate equilibrium between mitochondrial fission and fusion events. Both excessive fragmentation and hyper-fusion can be indicators of cellular stress. We observed a ~50% RNA editing level at the *C*-to-*T* recoding site and ~20% editing at the *A*-to-*G* site of *MFN1* in normal brain samples (Fig. 4A), which appears to be conserved in mice (fig. S8A). We hypothesize that an intermediate level of RNA editing is important in maintaining the balance between mitochondrial fusion and fission, since higher or lower RNA editing may disrupt this balance and alter mitochondria morphology and function. We observed that the edited versions of the MFN1 protein generally led to reduced mitochondrial fusion, relative to the unedited protein, in both human and mouse cells, highlighting the functional relevance of the two RNA editing sites. The observed reduced *MFN1* editing in SCZ may contribute to disease etiology. Alternatively, it may represent a mechanism by which the cell responds to stress stimuli arising from the disease. For example, one explanation may be that lower editing in SCZ, leading to hyperfusion upon cellular stress, may be a compensatory mechanism by which the cell attempts to protect against mitochondrial fragmentation, which leads to apoptosis, in SCZ brains (*27*). In vivo experiments in mice or other animal models are needed to test this conjecture.

Together, this work presents explicit evidence of the robust hypoediting trend in Europeans with SCZ and supports the functional relevance of RNA editing in nuclear encoded mitochondrial genes. Although we cannot determine the contribution of RNA editing to disease causality, we observed many functional pathways harboring various editing events that may contribute to disease risk (e.g., synaptic transmission and glutamate receptor activity). The large set of de novo editing sites resulting from our study will allow further elucidation of RNA editing differences observed in different ancestral groups. Together, our study provides an extensive characterization of RNA editing in SCZ and supplies valuable insight into the roles of dysregulated editing in mitochondrial function.

MATERIALS AND METHODS

RNA-seq datasets from PsychENCODE

RNA-seq data from the brain FC or dorsolateral prefrontal cortex (DLPFC) region were extracted from four cohorts in the PsychENCODE consortium: BrainGVEX, CMC, HBCC, and LIBD (table S1) (*25*). We followed strict quality control procedures to remove sample outliers in RIN, PMI, age, and other biological and technical variables (*19*). Retained SCZ and control groups did not differ significantly in any biological or technical covariables (figs. S2 and S4). The quality control procedure was conducted for European and African American samples separately in the HBCC and LIBD

cohorts. All downstream analyses were conducted on each cohort and ethnicity separately to validate our findings between cohorts and to limit noise due to potential cohort-specific batch effects. Final cohort sizes and number of case and control samples are provided in table S1.

Identification and annotation of RNA editing sites

RNA-seq was mapped using hisat2 (*51*) to the human reference genome with default parameters, except allowing no mixed or discordantly mapped reads (--no-mixed, --no-discordant). Only uniquely mapped read pairs were used for downstream analysis. Unmapped reads can often be generated from regions with clusters of editing sites (i.e., "hyper-edited" regions) that fail to map due to copious mismatches. We applied a previously developed method to alleviate this issue (*18*, *19*). Briefly, all adenosines in unmapped reads and the reference genome were converted to guanosines. This was followed by hisat2 alignment as described above and then restoration of the original adenosines in the reads. Uniquely mapped reads from this step were combined with the originally mapped reads and used in the following RNA editing analysis.

RNA editing sites were identified using methods previously developed by our group (*15*–*17*). Several filters were applied to remove loci resulting from spurious read mapping or sequencing errors (*16*). Editing sites were supported by at least five samples, in which each was required to have at least two edited reads and five total reads. The loci occurring in at least 10% of samples within a cohort were labeled as common RNA editing sites and used for downstream differential analysis (see below). Annotations of the genomic regions and host genes of RNA editing sites were obtained with the BiomaRt R package and Ensembl gene annotation (*52*, *53*). The ANNOVAR (*54*) software was used to label the functional categories of RNA editing sites. Last, editing sites were overlapped with Alu regions from RepeatMasker (*55*).

Differential RNA editing analysis

Differential RNA editing analysis was conducted for each cohort separately. To this end, we used a method previously developed in our laboratory that uncovers sites with either (*1*) significantly different average editing levels between SCZ and controls or (*2*) differential editing prevalence between the two conditions (*19*). As described below, this method adopts a strategy to allow a flexible read coverage requirement for each editing site, to adapt to the different total read coverage available to specific sites (*19*).

For each editing site e_i, we first identified the highest coverage possible (between a coverage of ≥20, 15, or 5 reads) at which there were a minimum of five samples per condition. After the highest possible read coverage C for e_i was chosen, we calculated separate average editing level per condition (A_{iSCZ} and $A_{iControl}$) using samples with a minimum of C coverage. We then considered samples that fulfilled lower read coverage thresholds (≥15, 10, or 5) and included these samples in A_{iSCZ} or $A_{iControl}$ only if their inclusion did not alter the average editing level by >0.03. A Wilcoxon rank sum test was conducted to detect the difference in editing levels between SCZ and control groups. If an initial read coverage requirement C was not reached, then we tested all samples where e_i had ≥5 read coverage for at least 20% SCZ and 20% control samples. Differential editing sites were those with Wilcoxon rank sum $P < 0.05$ and an effect size > 5%.

To identify differential editing sites that had significantly different editing prevalence between SCZ and controls, we used a Fisher's exact test to compare the total numbers of SCZ and control samples with nonzero editing level versus zero editing level, as previously described by Tran *et al.* (*19*). The adaptive procedure for minimum read coverage requirements described above was also applied here. Editing sites with differential prevalence between the groups were those with $P < 0.05$ and an effect size > 5%.

DREA was calculated per sample using the mean editing level across all differential editing sites with read coverage ≥ 5 reads. A Wilcoxon rank sum test was conducted to determine the significance of overall DREA trend between SCZ and control. Heatmaps of differential editing levels throughout the study were generated with the R package gplots (*56*).

Weighted gene coexpression network analysis

We detected clusters of loci whose editing levels associated with SCZ diagnosis using the WGCNA package (*26*) in R for the BrainGVEX and CMC cohorts separately. We focused on common editing sites and those that showed large variations across samples. Specifically, an RNA editing site was considered testable in the cohort if (i) it was labeled as common in the cohort (defined above), (ii) it had ≥5 reads in ≥90% of samples, and (iii) its editing levels had an SD > 0.1 across samples. WGCNA was conducted using automatic network construction and module detection, for which the soft threshold powers were set to be 2 or 3 for the BrainGVEX or CMC cohorts, respectively, to fit a scale-free topology (*26*).

The WGCNA network construction and consensus modules were chosen using the blockwiseConsensusModules function with default parameters, except for the soft threshold powers mentioned above. The eigengenes of each module were correlated with condition to identify the module most relevant to disease status. This correlation was conducted using a linear regression model, where biological (age and gender) and technical covariates (RIN, PMI, and total reads) were included. The largest module (the turquoise module) significantly associated with disease status in both BrainGVEX and CMC (fig. S7).

GO enrichment of genes of interest

GO terms were obtained for a query gene set using the R package BiomaRt and Ensembl annotation (*52*, *53*). For each query gene, we randomly picked a control gene with matched gene expression and gene length (±10% relative to that of the query gene). The controls of all query genes constitute one set of control genes. This process was repeated 10,000 times. Query genes without a matched control were excluded from the analysis. For each GO term, the number of its occurrences in the 10,000 sets of random controls was fit into a Gaussian distribution. The frequency of the term in the query gene set was then compared to this distribution to obtain an enrichment P value. Only terms that contain at least two genes in the query were considered. In rare cases, a particular GO term does not occur in the control sets. Its P value was set to 1×10^{-100} for visualization purposes.

Cell type proportion from bulk RNA-seq

Fragments per kilobase of exon per million reads mapped (FPKM) for bulk RNA-seq was calculated on the basis of read counts per gene obtained using the HTSeq software (*57*) and total mapped reads from hisat2 (*58*). Cell type proportion for five main cell

types in the human brain (neurons, astrocytes, oligodendrocytes, microglia, and endothelial cells) was estimated using the "impute cell fractions" method in the CIBERSORTx software (*23*). CIBERSORTx was provided with bulk gene expression and a cell type signature matrix of genes, which was derived from single-cell RNA-seq of human PFC in previous studies (*28*, *59*). After obtaining normalized cell type proportion values for each sample and cell type, we conducted Wilcoxon rank sum tests between conditions for each cell type to determine differences in proportion. Cell types with FDR adjusted $P < 0.05$ were marked with red asterisks (figs. S1J and S5B).

Cell type–specific DREA

Cell type–specific DREA was calculated by taking the average editing level of all differential editing sites located in the signature genes of a cell type. Differential editing sites with at least five reads were included. A Wilcoxon rank sum test was conducted between conditions to ascertain cell type DREA differences (red asterisk denoting FDR adjusted $P < 0.05$; figs. S1K and S5C).

Single-nucleus RNA-seq data and RNA editing quantification

We obtained previously published single-nucleus transcriptomes of six major brain cell types—neurons (both excitatory and inhibitory), astrocytes, oligodendrocytes, microglia, endothelial, and OPCs—from the PFC of 24 control subjects (*22*). Data of the same cell type were combined for RNA editing detection and transcripts per million (TPM) calculation, which were conducted similarly as described above.

For each cell type in each sample, we estimated the fraction of genes expressed with TPM ≥ 5 among all differentially edited genes in the BrainGVEX cohort (Fig. 1G). In addition, we estimated the fraction of differentially edited sites in the BrainGVEX cohort that have detectable editing in each cell type. That is, for each cell type in each sample, we obtained the ratio between the number of detected RNA editing sites and the total differential editing sites in BrainGVEX (Fig. 1H).

MPRA of 3′UTR differential editing sites

A total of 770 differential *A*-to-*G* editing sites located in 3′UTRs from the BrainGVEX, CMC, HBCC, or LIBD data were included in the MPRA experiment in HEK293 cells. Specifically, we synthesized 200 nt-long oligos (Twist Biosciences) containing cloning adaptors and 158 nt-long test sequences with the editing site at the center of the test region. If the editing site is close to either boundary of the 3′UTR, then the flanking regions of the editing site were adjusted such that the 158 nt-long test sequence resided within the 3′UTR. The edited (G) and unedited (A) versions of the editing sites were both synthesized. The test sequences were cloned into the 3′UTR of the *eGFP* gene in the master plasmids. The plasmid library was then electroporated into HEK293 cells followed by RNA extraction 24 hours after cell transfection. Last, the test sequences were amplified from both plasmid library and mRNA to generate DNA sequencing and RNA-seq libraries, similarly as in previous MPRA experiments (*60*, *61*). Three biological replicates were collected for each experiment, and a high correlation was observed between replicates ($R = 0.84$). Sequencing data of the plasmid DNA and mRNA were compared to identify sites associated with significant expression differences between the two alleles (*A* and *G*) using MPRAnalyze (*62*). FDR ≤ 0.1 and |ln(Fold Change)| ≥ 0.1 were required to call significance.

Correlation between 3′UTR editing and gene expression

For each differential editing site in the 3′UTR, we correlated the editing levels and the expression levels of the host gene (log FPKM) across all samples, using a linear regression model that included sample PMI, RIN, age of death, and sex as covariates. Only sites with ≥5 reads in ≥10 samples were deemed to be testable. This analysis was conducted for each of the four cohorts separately. However, FDR correction was applied to *P* values obtained from all cohorts combined. The *t*-statistic, the number of SDs by which the correlation deviated from zero, was used to determine association directionality for visualization (Fig. 3C).

Gene regulatory network of EdEx genes

We used GeneMANIA (*30*) to obtain known genetic interactions for 195 genes whose 3′UTR differential editing sites were significantly associated with their respective gene expression. GeneMANIA identified 20 additional genes strongly connected with the 195 genes through its database of known networks. The gene regulatory network encompassing 215 genes was visualized using Cytoscape v3.8.2 (*31*). GO enrichment was conducted for the 195 genes to identify functional categories. Genes that fell into similar categories were grouped together in the network visualization. FDR-corrected *P* values (*q* values) for the GO categories were labeled on the network. For those categories with multiple GO terms, the most significant *q* value was shown (Fig. 3E).

MFN1 editing in zebrafish

RNA-seq extracted from zebrafish (*Danio rerio*) brain tissue was obtained from Wong and Godwin (*35*) using the National Center for Biotechnology Information's Gene Expression Omnibus database (GSE61108). The neurotranscriptome profiles for a total of four strains and 160 samples were analyzed. Same-sex individuals were pooled into a biological replicate. A total of 16 RNA-seq datasets (two biological replicates from each sex for each strain) were mapped to genome assembly GRCz11 using the hisat2 (*51*) software as described previously. Editing ratios for orthologous *MFN1* sites (*mfn1b* in zebrafish) were manually calculated on the basis of the integrative genomics viewer (*63*).

Cell culture

Mfn1 and *Mfn2* dKO MEFs were gifted by D. Chan (California Institute of Technology). HEK293 cells were gifted by J. Huang [University of California, Los Angeles (UCLA)]. Mouse neuro2a (N2a) and HEK293T cells were obtained from American Type Culture Collection. Cells were maintained with Dulbecco's modified Eagle's medium (DMEM; Gibco, 10569010) supplemented with 10% fetal bovine serum (Gibco, 10082147) and 1× antibiotic-antimycotics (Gibco, 15240096) at 37°C and 5% CO_2. For the neuronal differentiation of N2a cells, the cells were seeded at 40 to 50% of density and grown for 24 hours in complete medium. Following this, the cells were washed with 1× Dulbecco's phosphate-buffered saline (DPBS; Gibco, 14190144) and then replaced in serum-free medium.

MFN1 editing constructs

Human and mouse *MFN1* constructs were gifted by O. Shirihai (UCLA). *MFN1* editing mutations were generated by the Q5 site directed mutagenesis kit (New England Biolabs, E0554S) and then cloned into pqCXIP (Clontech, 631516) for stable *Mfn1* expression in MEF cells.

RNA isolation, RT-PCR amplification, and analysis of RNA editing

Cultured cells and brain tissues were homogenized in TRIzol (Thermo Fisher Scientific, 15596018). The mixture was incubated on ice for 15 min. Chloroform was added to the mixture and incubated at room temperature for 10 min. The mixture was centrifuged at 12,000*g* for 15 min, and the top layer was carefully extracted. An equal volume of 100% ethanol was added to the top chloroform layer and mixed thoroughly. Total RNA of N2a cells was also extracted using the TRIzol reagent. RNA was further purified using the Direct-zol RNA MiniPrep Plus kit (Zymo Research, R2072) according to the manufacturer′s protocol. Reverse transcription was performed on 1 μg of total RNA for 1 hour at 42°C using random hexamer primer and SuperScript IV (Thermo Fisher Scientific, 18090050). The cDNA product was detected by polymerase chain reaction (PCR) using the *Mfn1* gene–specific primer set. Amplification was performed for 30 cycles, consisting of 30s at 95°C, 30s at 55°C, and 1 min at 72°C. The products from reverse transcription (RT)–PCR were resolved on 1% agarose gels. The appropriate PCR product was excised, and the DNA was extracted, purified, and analyzed by Sanger sequencing. *C*-to-*T* editing levels were calculated as relative peak heights [that is, ratio between the *T* peak height and the combined height of *C* and *T* peaks: height *T*/(height *C* + height *T*)].

TOPO cloning and clonal sequencing

PCR products were run on 1% agarose gel and visualized under ultraviolet light. The band with the expected size was isolated by a Zymoclean Gel DNA Recovery kit (Zymo Research, D4002) according to the manufacturer′s protocol. The PCR product was inserted into kanamycin-resistant pCR 2.1-TOPO vector (Thermo Fisher Scientific, 450641). Ligated clones were transformed into One Shot TOP10 Chemically Competent *Escherichia coli* (Thermo Fisher Scientific, C404003). Transformed cells were streaked on LB agar plates containing kanamycin and X-Gal as selection markers and incubated overnight at 37°C. Ten white colonies were randomly selected, and each colony was inoculated overnight in LB containing kanamycin. Plasmid was extracted using Plasmid DNA Miniprep Kits (Thermo Fisher Scientific, K210011). Miniprep samples were subject to Sanger sequencing. The number of clones presenting a thiamine (T, representing C > U editing) or guanine (G, representing A > I editing) peak at the editing sites in the *Mfn1* gene was counted to determine the editing ratio.

Production of lentivirus and cell transduction for protein knockdown

Constructs containing pLKO1 nontarget control short hairpin RNA (shRNA; SHC016), *Apobec1*-targeting shRNA (TRCN0000311145), *Apobec2*-targeting shRNA (TRCN0000112015), or *Apobec3*-targeting shRNA (TRCN0000197906) were used. We produced lentiviruses via cotransfection of pCMV-d8.91, pVSV-G, and pLKO1 into HEK293T cells using Lipofectamine 3000 (Thermo Fisher Scientific, L3000015). Transduction was carried out according to the standard protocol of the ENCODE consortium. Briefly, viruses were collected from conditioned media after 48-hour cotransfection. Lentivirus-containing medium was mixed with the same volume of DMEM containing polybrene (8 μg/ml), which was used to infect N2a cells. After 24 hours, cells were incubated with puromycin (3 μg/m) for 24 hours. Knockdown efficiency was evaluated by real-time quantitative PCR (Bio-Rad).

Analysis of mitochondrial morphology

Mfn1 and *Mfn2* dKO MEF cells were seeded and incubated for 24 hours in 384-well plates (E&K Scientific, EK-30091) and then stained with 200 nM MitoTracker Green FM (Invitrogen, M7514) for 30 min at 37°C. Mitochondria were visualized with the Zeiss LSM 780 confocal microscope and ZEN software (Zeiss).

PI staining

Cells were stained using PI (1 μg/ml; Invitrogen, V13242) and Hoechst 33342 (1 μg/ml; Invitrogen, H3570) for 10 min. Images were obtained using confocal microscopy and analyzed by the ImageJ software (http://imagej.nih.gov/ij/).

Mitochondrial fractionation

Mitochondrial and cytosol fractions were isolated using the mitochondria isolation kit for cultured cells (Thermo Fisher Scientific, 89874). Briefly, 80% confluent cells in a 10-cm culture dish were resuspended in 800 μl of reagent A and incubated for 2 min on ice. Then, 10 μl reagent B was mixed by vortexing for 5 min. Samples were mixed with 800-μl reagent C and centrifuged at 700*g* for 10 min at 4°C. The supernatant was transferred to a new tube and centrifuged at 12,000*g* for 15 min at 4°C. The supernatant was then collected as the cytosol fraction. The mitochondrial fraction in the pellet was washed once with 500-μl DPBS and centrifuged at 12,000*g* for 5 min at 4°C. The mitochondrial fraction was dissolved in 200-μl DPBS with sonication at 25% amplitude for 10 s (twice) with an Ultrasonic Processor 120 W, 20 kHz (Thermo Fisher Scientific).

Western blot

Cells were lysed and separated via the Novex NuPAGE system (Invitrogen, NP0008, NP0001, and LC3675) and the ExpressPlus PAGE Gel (GenScript). Polyvinylidene difluoride membranes (Millipore, IPVH304F0) were used for transfer and then probed with the following primary antibodies in 3% bovine serum albumin/Tris-buffered saline with 0.1% Tween 20 detergent (TBST): β-tubulin (Santa Cruz Biotechnology, sc-23949), adenosine triphosphate synthase 5 alpha (ATP5a) (Abcam, ab14748), Cyt C (Santa Cruz Biotechnology, sc-13156), MFN1 (Abcam, ab57602), MFN2 (Abcam, ab56889), and β-actin (Santa Cruz Biotechnology, sc-47778). The antibodies were detected using horseradish peroxidase–conjugated antibodies (Invitrogen, 31430), the ECL Prime Western Blotting System (GE HealthCare, RPN2232), and the Syngene Pxi Imager.

MFN1 genome editing

We introduced *MFN1* editing sites to the genome of HEK293T cells via Prime editing (*38*). The spacer and extension sequences were designed according to the guidelines provided previously (*38*). The designed oligos were cloned into the pU6-pegRNA-GG-

acceptor (Addgene, 132777) to generate both pegRNA and nick guide RNA (gRNA) expressing constructs (oligo sequences were listed in table S4). Plasmids expressing pegRNA (250 ng), nick gRNA (83 ng), and prime editor (750 ng), namely, pCMV-PE2 (Addgene, 132775), were cotransfected into HEK293T (7500 cells per well in 48-well plates) with Lipofectamine 3000 Transfection Reagent (Thermo Fisher Scientific, catalog no. L3000015) according to the manufacturer's protocol. After 72 hours, genomic DNA was extracted, amplified by PCR, and sequenced via Sanger sequencing to confirm genome editing events. To optimize the editing efficiency, different combinations of pegRNAs and nick gRNAs (PE2, PE3, and PE3b) were tested. The prime binding site (PBS) and RT template were also optimized to 9 nt for PBS and 19 nt for RT template. The optimal condition (PE3b, 9-nt PBS, and 19-nt RT template) was used in scaled-up experiments to generate single-cell clones with *MFN1* genome editing by serial dilution.

Mitochondria hyperfusion test

HEK293T cells were seeded on the four-chambered coverglass (Nunc, Lab-TekII). Cycloheximide (10 μM) was added to 70% confluent cells for 30 min and then stained with MitoTracker Green FM (Invitrogen, M7514) for 30 min at 37°C. Mitochondria images were obtained using the Leica DMI-4000 confocal microscope and Leica application suite software. The mitochondrial hyperfusion score was calculated as described previously (*39*).

Statistics for *MFN1*-related experimental data

GraphPad Prism 9 was used for statistical analysis and graphical display of the data. All graphs represent mean ± SEM. Statistical tests and significance values were indicated in the figure legends.

Supplementary Materials

This PDF file includes:
Figs. S1 to S8
Legends for tables S1 to S4

Other Supplementary Material for this manuscript includes the following:
Tables S1 to S4

View/request a protocol for this paper from *Bio-protocol*.

REFERENCES AND NOTES

1. K. Nishikura, A-to-I editing of coding and non-coding RNAs by ADARs. *Nat. Rev. Mol. Cell Biol.* **17**, 83–96 (2016).
2. J. D. Salter, R. P. Bennett, H. C. Smith, The APOBEC protein family: United by structure, divergent in function. *Trends Biochem. Sci.* **41**, 578–594 (2016).
3. C. R. Walkley, J. B. Li, Rewriting the transcriptome: Adenosine-to-inosine RNA editing by ADARs. *Genome Biol.* **18**, 205 (2017).
4. Y. H. E. Hsiao, J. H. Bahn, Y. Yang, X. Lin, S. Tran, E. W. Yang, G. Quinones-Valdez, X. Xiao, RNA editing in nascent RNA affects pre-mRNA splicing. *Genome Res.* **28**, 812–823 (2018).
5. A. Brümmer, Y. Yang, T. W. Chan, X. Xiao, Structure-mediated modulation of mRNA abundance by A-to-I editing. *Nat. Commun.* **8**, 1255 (2017).
6. L. Bazak, A. Haviv, M. Barak, J. Jacob-Hirsch, P. Deng, R. Zhang, F. J. Isaacs, G. Rechavi, J. B. Li, E. Eisenberg, E. Y. Levanon, A-to-I RNA editing occurs at over a hundred million genomic sites, located in a majority of human genes. *Genome Res.* **24**, 365–376 (2014).
7. J. B. Li, G. M. Church, Deciphering the functions and regulation of brain-enriched A-to-I RNA editing. *Nat. Neurosci.* **16**, 1518–1522 (2013).
8. M. S. Breen, A. Dobbyn, Q. Li, P. Roussos, G. E. Hoffman, E. Stahl, A. Chess, P. Sklar, J. B. Li, B. Devlin, J. D. Buxbaum, S. Akbarian, J. Bendl, K. Brennand, L. Brown, A. Browne, A. Charney, L. Couto, G. Crawford, O. Devillers, E. Domenici, M. Filosi, E. Flatow, N. Francoeur, J. F. Fullard, S. E. Gil, K. Girdhar, A. Gulyás-Kovács, R. Gur, C. G. Hahn, V. Haroutunian, M. E. Hauberg, L. Huckins, R. Jacobov, Y. Jiang, J. S. Johnson, B. Kassim, Y. Kim, L. Klei, R. Kramer, M. Lauria, T. Lehner, D. A. Lewis, B. K. Lipska, S. Marenco, L. M. Mangravite, K. Montgomery, R. Park, T. M. Perumal, M. A. Peters, C. Rosenbluh, D. M. Ruderfer, G. Senthil, H. R. Shah, S. K. Sieberts, L. Sloofman, L. Song, P. Sullivan, R. Visintainer, J. Wang, Y. C. Wang, J. Wiseman, E. Xia, W. Zhang, E. Zharovsky, Global landscape and genetic regulation of RNA editing in cortical samples from individuals with schizophrenia. *Nat. Neurosci.* **22**, 1402–1412 (2019).
9. R. A. McCutcheon, T. Reis Marques, O. D. Howes, Schizophrenia—An overview. *JAMA Psychiatry* **77**, 201–210 (2020).
10. C. A. Ross, R. L. Margolis, S. A. J. Reading, M. Pletnikov, J. T. Coyle, Neurobiology of schizophrenia. *Neuron* **52**, 139–153 (2006).
11. V. Trubetskoy, A. F. Pardiñas, T. Qi, G. Panagiotaropoulou, S. Awasthi, T. B. Bigdeli, J. Bryois, C.-Y. Chen, C. A. Dennison, L. S. Hall, M. Lam, K. Watanabe, O. Frei, T. Ge, J. C. Harwood, F. Koopmans, S. Magnusson, A. L. Richards, J. Sidorenko, Y. Wu, J. Zeng, J. Grove, M. Kim, Z. Li, G. Voloudakis, W. Zhang, M. Adams, I. Agartz, E. G. Atkinson, E. Agerbo, M. A. Eissa, M. Albus, M. Alexander, B. Z. Alizadeh, K. Alptekin, T. D. Als, F. Amin, V. Arolt, M. Arrojo, L. Athanasiu, M. H. Azevedo, S. A. Bacanu, N. J. Bass, M. Begemann, R. A. Belliveau, J. Bene, B. Benyamin, S. E. Bergen, G. Blasi, J. Bobes, S. Bonassi, A. Braun, R. A. Bressan, E. J. Bromet, R. Bruggeman, P. F. Buckley, R. L. Buckner, J. Bybjerg-Grauholm, W. Cahn, M. J. Cairns, M. E. Calkins, V. J. Carr, D. Castle, S. V. Catts, K. D. Chambert, R. C. K. Chan, B. Chaumette, W. Cheng, E. F. C. Cheung, S. A. Chong, D. Cohen, A. Consoli, Q. Cordeiro, J. Costas, C. Curtis, M. Davidson, K. L. Davis, L. de Haan, F. Degenhardt, L. E. De Lisi, D. Demontis, F. Dickerson, D. Dikeos, T. Dinan, S. Djurovic, J. Duan, G. Ducci, F. Dudbridge, J. G. Eriksson, L. Fañanás, S. V. Faraone, A. Fiorentino, A. Forstner, J. Frank, N. B. Freimer, M. Fromer, A. Frustaci, A. Gadelha, G. Genovese, E. S. Gershon, M. Giannitelli, I. Giegling, P. Giusti-Rodríguez, S. Godard, J. I. Goldstein, J. G. Peñas, A. González-Pinto, S. Gopal, J. Gratten, M. F. Green, T. A. Greenwood, O. Guillin, S. Gülöksüz, R. E. Gur, R. C. Gur, B. Gutiérrez, E. Hahn, H. Hakonarson, V. Haroutunian, A. M. Hartmann, C. Harvey, C. Hayward, F. A. Henskens, S. Herms, P. Hoffmann, D. P. Howrigan, M. Ikeda, C. Iyegbe, I. Joa, A. Julià, A. K. Kähler, T. Kam-Thong, Y. Kamatani, S. Karachanak-Yankova, O. Kebir, M. C. Keller, B. J. Kelly, A. Khrunin, S.-W. Kim, J. Klovins, N. Kondratiev, B. Konte, J. Kraft, M. Kubo, V. Kučinskas, Z. A. Kučinskiene, A. Kusumawardhani, H. Kuzelova-Ptackova, S. Landi, L. C. Lazzeroni, P. H. Lee, S. E. Legge, D. S. Lehrer, R. Lencer, B. Lerer, M. Li, J. Lieberman, G. A. Light, S. Limborska, C.-M. Liu, J. Lönnqvist, C. M. Loughland, J. Lubinski, J. J. Luykx, A. Lynham, M. M. Jr, A. Mackinnon, P. K. E. Magnusson, B. S. Maher, W. Maier, D. Malaspina, J. Mallet, S. R. Marder, S. Marsal, A. R. Martin, L. Martorell, M. Mattheisen, R. W. McCarley, C. M. Donald, J. J. McGrath, H. Medeiros, S. Meier, B. Melegh, I. Melle, R. I. Mesholam-Gately, A. Metspalu, P. T. Michie, L. Milani, V. Milanova, M. Mitjans, E. Molden, E. Molina, M. D. Molto, V. Mondelli, C. Moreno, C. P. Morley, G. Muntané, K. C. Murphy, I. Myin-Germeys, I. Nenadić, G. Nestadt, L. Nikitina-Zake, C. Noto, K. H. Nuechterlein, N. L. O'Brien, F. A. O'Neill, S.-Y. Oh, A. Olincy, V. K. Ota, C. Pantelis, G. N. Papadimitriou, M. Parellada, T. Paunio, R. Pellegrino, S. Periyasamy, D. O. Perkins, B. Pfuhlmann, O. Pietiläinen, J. Pimm, D. Porteous, J. Powell, D. Quattrone, D. Quested, A. D. Radant, A. Rampino, M. H. Rapaport, A. Rautanen, A. Reichenberg, C. Roe, J. L. Roffman, J. Roth, M. Rothermundt, B. P. F. Rutten, S. Saker-Delye, V. Salomaa, J. Sanjuan, M. L. Santoro, A. Savitz, U. Schall, R. J. Scott, L. J. Seidman, S. I. Sharp, J. Shi, L. J. Siever, E. Sigurdsson, K. Sim, N. Skarabis, P. Slominsky, H.-C. So, J. L. Sobell, E. Söderman, H. J. Stain, N. E. Steen, A. A. Steixner-Kumar, E. Stögmann, W. S. Stone, R. E. Straub, F. Streit, E. Strengman, T. S. Stroup, M. Subramaniam, C. A. Sugar, J. Suvisaari, D. M. Svrakic, N. R. Swerdlow, J. P. Szatkiewicz, T. M. T. Ta, A. Takahashi, C. Terao, F. Thibaut, D. Toncheva, P. A. Tooney, S. Torretta, S. Tosato, G. B. Tura, B. I. Turetsky, A. Üçok, A. Vaaler, T. van Amelsvoort, R. van Winkel, J. Veijola, J. Waddington, H. Walter, A. Waterreus, B. T. Webb, M. Weiser, N. M. Williams, S. H. Witt, B. K. Wormley, J. Q. Wu, Z. Xu, R. Yolken, C. C. Zai, W. Zhou, F. Zhu, F. Zimprich, E. C. Atbaşoğlu, M. Ayub, C. Benner, A. Bertolino, D. W. Black, N. J. Bray, G. Breen, N. G. Buccola, W. F. Byerley, W. J. Chen, C. R. Cloninger, B. Crespo-Facorro, G. Donohoe, R. Freedman, C. Galletly, M. J. Gandal, M. Gennarelli, D. M. Hougaard, H.-G. Hwu, A. V. Jablensky, S. A. McCarroll, J. L. Moran, O. Mors, P. B. Mortensen, B. Müller-Myhsok, A. L. Neil, M. Nordentoft, M. T. Pato, T. L. Petryshen, M. Pirinen, A. E. Pulver, T. G. Schulze, J. M. Silverman, J. W. Smoller, E. A. Stahl, D. W. Tsuang, E. Vilella, S.-H. Wang, S. Xu; Indonesia Schizophrenia Consortium; PsychENCODE; Psychosis Endophenotypes International Consortium; SynGO Consortium, R. Adolfsson, C. Arango, B. T. Baune, S. I. Belangero, A. D. Børglum, D. Braff, E. Bramon, J. D. Buxbaum, D. Campion, J. A. Cervilla, S. Cichon, D. A. Collier, A. Corvin, D. Curtis, M. D. Forti, E. Domenici, H. Ehrenreich, V. Escott-Price, T. Esko, A. H. Fanous, A. Gareeva, M. Gawlik, P. V. Gejman, M. Gill, S. J. Glatt, V. Golimbet, K. S. Hong, C. M. Hultman, S. E. Hyman, N. Iwata, E. G. Jönsson, R. S. Kahn, J. L. Kennedy, E. Khusnutdinova, G. Kirov, J. A. Knowles, M.-O. Krebs, C. Laurent-Levinson, J. Lee, T. Lencz, D. F. Levinson, Q. S. Li, J. Liu, A. K. Malhotra, D. Malhotra, A. M. Intosh, A. M. Quillin, P. R. Menezes, V. A. Morgan, D. W. Morris, B. J. Mowry, R. M. Murray, V. Nimgaonkar, M. M. Nöthen, R. A. Ophoff, S. A. Paciga, A. Palotie, C. N. Pato, S. Qin, M. Rietschel, B. P. Riley, M. Rivera, D. Rujescu, M. C. Saka, A. R. Sanders, S. G. Schwab,

A. Serretti, P. C. Sham, Y. Shi, D. S. Clair, H. Stefánsson, K. Stefansson, M. T. Tsuang, J. van Os, M. P. Vawter, D. R. Weinberger, T. Werge, D. B. Wildenauer, X. Yu, W. Yue, P. A. Holmans, A. J. Pocklington, P. Roussos, E. Vassos, M. Verhage, P. M. Visscher, J. Yang, D. Posthuma, O. A. Andreassen, K. S. Kendler, M. J. Owen, N. R. Wray, M. J. Daly, H. Huang, B. M. Neale, P. F. Sullivan, S. Ripke, J. T. R. Walters, M. C. O'Donovan; Schizophrenia Working Group of the Psychiatric Genomics Consortium, Mapping genomic loci implicates genes and synaptic biology in schizophrenia. *Nature* **604**, 502–508 (2022).

12. G. Silberberg, D. Lundin, R. Navon, M. Öhman, Deregulation of the A-to-I RNA editing mechanism in psychiatric disorders. *Hum. Mol. Genet.* **21**, 311–321 (2012).
13. M. J. Gandal, J. R. Haney, N. N. Parikshak, V. Leppa, G. Ramaswami, C. Hartl, A. J. Schork, V. Appadurai, A. Buil, T. M. Werge, C. Liu, K. P. White; Commonmind Consortium; Psychencode Consortium; IPSYCH-Broad Working Group, S. Horvath, D. H. Geschwind, Shared molecular neuropathology across major psychiatric disorders parallels polygenic overlap. *Science* **359**, 693–697 (2018).
14. S. Akbarian, C. Liu, J. A. Knowles, F. M. Vaccarino, P. J. Farnham, G. E. Crawford, A. E. Jaffe, D. Pinto, S. Dracheva, D. H. Geschwind, J. Mill, A. C. Nairn, A. Abyzov, S. Pochareddy, S. Prabhakar, S. Weissman, P. F. Sullivan, M. W. State, Z. Weng, M. A. Peters, K. P. White, M. B. Gerstein, A. Amiri, C. Armoskus, A. E. Ashley-Koch, T. Bae, A. Beckel-Mitchener, B. P. Berman, G. A. Coetzee, G. Coppola, N. Francoeur, M. Fromer, R. Gao, K. Grennan, J. Herstein, D. H. Kavanagh, N. A. Ivanov, Y. Jiang, R. R. Kitchen, A. Kozlenkov, M. Kundakovic, M. Li, Z. Li, S. Liu, L. M. Mangravite, E. Mattei, E. Markenscoff-Papadimitriou, F. C. P. Navarro, N. North, L. Omberg, D. Panchision, N. Parikshak, J. Poschmann, A. J. Price, M. Purcaro, T. E. Reddy, P. Roussos, S. Schreiner, S. Scuderi, R. Sebra, M. Shibata, A. W. Shieh, M. Skarica, W. Sun, V. Swarup, A. Thomas, J. Tsuji, H. van Bakel, D. Wang, Y. Wang, K. Wang, D. M. Werling, A. J. Willsey, H. Witt, H. Won, C. C. Y. Wong, G. A. Wray, E. Y. Wu, X. Xu, L. Yao, G. Senthil, T. Lehner, P. Sklar, N. Sestan, The PsychENCODE project. *Nat. Neurosci.* **18**, 1707–1712 (2015).
15. J. H. Bahn, J.-H. Lee, G. Li, C. Greer, G. Peng, X. Xiao, Accurate identification of A-to-I RNA editing in human by transcriptome sequencing. *Genome Res.* **22**, 142–150 (2012).
16. J.-H. Lee, J. K. Ang, X. Xiao, Analysis and design of RNA sequencing experiments for identifying RNA editing and other single-nucleotide variants. *RNA.* **19**, 725–732 (2013).
17. Q. Zhang, X. Xiao, Genome sequence-independent identification of RNA editing sites. *Nat. Methods* **12**, 347–350 (2015).
18. H. T. Porath, S. Carmi, E. Y. Levanon, A genome-wide map of hyper-edited RNA reveals numerous new sites. *Nat. Commun.* **5**, 4726 (2014).
19. S. S. Tran, H.-I. Jun, J. H. Bahn, A. Azghadi, G. Ramaswami, E. L. Van Nostrand, T. B. Nguyen, Y.-H. E. Hsiao, C. Lee, G. A. Pratt, V. Martínez-Cerdeño, R. J. Hagerman, G. W. Yeo, D. H. Geschwind, X. Xiao, Widespread RNA editing dysregulation in brains from autistic individuals. *Nat. Neurosci.* **22**, 25–36 (2019).
20. E. Picardi, A. M. D'Erchia, C. Lo Giudice, G. Pesole, REDIportal: A comprehensive database of A-to-I RNA editing events in humans. *Nucleic Acids Res.* **45**, D750–D757 (2017).
21. D. Harjanto, T. Papamarkou, C. J. Oates, V. Rayon-Estrada, F. N. Papavasiliou, A. Papavasiliou, RNA editing generates cellular subsets with diverse sequence within populations. *Nat. Commun.* **7**, 12145 (2016).
22. H. Mathys, J. Davila-Velderrain, Z. Peng, F. Gao, S. Mohammadi, J. Z. Young, M. Menon, L. He, F. Abdurrob, X. Jiang, A. J. Martorell, R. M. Ransohoff, B. P. Hafler, D. A. Bennett, M. Kellis, L. H. Tsai, Single-cell transcriptomic analysis of Alzheimer's disease. *Nature* **570**, 332–337 (2019).
23. A. M. Newman, C. B. Steen, C. L. Liu, A. J. Gentles, A. A. Chaudhuri, F. Scherer, M. S. Khodadoust, M. S. Esfahani, B. A. Luca, D. Steiner, M. Diehn, A. A. Alizadeh, Determining cell type abundance and expression from bulk tissues with digital cytometry. *Nat. Biotechnol.* **37**, 773–782 (2019).
24. Q. Yu, Z. He, Comprehensive investigation of temporal and autism-associated cell type composition-dependent and independent gene expression changes in human brains. *Sci. Rep.* **7**, 4121 (2017).
25. D. Wang, S. Liu, J. Warrell, H. Won, X. Shi, F. C. P. Navarro, D. Clarke, M. Gu, P. Emani, Y. T. Yang, X. Min, M. J. Gandal, S. Lou, J. Zhang, J. J. Park, C. Yan, S. KyongRhie, K. Manakongtreecheep, H. Zhou, A. A. Natha, M. Peters, E. Mattei, D. Fitzgerald, T. Brunetti, J. Moore, Y. Jiang, K. Girdhar, G. E. Hoffman, S. Kalayci, Z. H. Gümüş, G. E. Crawford, P. Roussos, S. Akbarian, A. E. Jaffe, K. P. White, Z. Weng, N. Sestan, D. H. Geschwind, J. A. Knowles, M. B. Gerstein, Comprehensive functional genomic resource and integrative model for the human brain. *Science* **362**, eaat8464 (2018).
26. P. Langfelder, S. Horvath, WGCNA: An R package for weighted correlation network analysis. *BMC Bioinformatics* **9**, 559 (2008).
27. K. H. Flippo, S. Strack, An emerging role for mitochondrial dynamics in Schizophrenia. *Schizophr. Res.* **187**, 26 (2017).
28. C. C. Yang, Y. T. Chen, Y. F. Chang, H. Liu, Y. P. Kuo, C. T. Shih, W. C. Liao, H. W. Chen, W. S. Tsai, B. C. M. Tan, ADAR1-mediated 3′ UTR editing and expression control of antiapoptosis genes fine-tunes cellular apoptosis response. *Cell Death Dis.* **8**, e2833 (2017).
29. D. A. Siegel, O. Le Tonqueze, A. Biton, N. Zaitlen, D. J. Erle, Massively parallel analysis of human 3′ UTRs reveals that AU-rich element length and registration predict mRNA destabilization. *G3 (Bethesda)* **12**, jkab404 (2022).
30. D. Warde-Farley, S. L. Donaldson, O. Comes, K. Zuberi, R. Badrawi, P. Chao, M. Franz, C. Grouios, F. Kazi, C. T. Lopes, A. Maitland, S. Mostafavi, J. Montojo, Q. Shao, G. Wright, G. D. Bader, Q. Morris, The GeneMANIA prediction server: Biological network integration for gene prioritization and predicting gene function. *Nucleic Acids Res.* **38**, W214–W220 (2010).
31. P. Shannon, A. Markiel, O. Ozier, N. S. Baliga, J. T. Wang, D. Ramage, N. Amin, B. Schwikowski, T. Ideker, Cytoscape: A software environment for integrated models of biomolecular interaction networks. *Genome Res.* **13**, 2498 (2003).
32. R. J. Youle, A. M. Van Der Bliek, Mitochondrial fission, fusion, and stress. *Science* **337**, 1062–1065 (2012).
33. L.-Q. Ye, H. Zhao, H.-J. Zhou, X.-D. Ren, L.-L. Liu, N. O. Otecko, Z. Wang, M.-M. Yang, L. Zeng, X.-T. Hu, Y.-G. Yao, Y.-P. Zhang, D.-D. Wu, The RNA editome of Macaca mulatta and functional characterization of RNA editing in mitochondria. *Sci. Bull.* **62**, 820–830 (2017).
34. P. Danecek, C. Nellåker, R. E. McIntyre, J. E. Buendia-Buendia, S. Bumpstead, C. P. Ponting, J. Flint, R. Durbin, T. M. Keane, D. J. Adams, High levels of RNA-editing site conservation amongst 15 laboratory mouse strains. *Genome Biol.* **13**, 1–12 (2012).
35. R. Y. Wong, J. Godwin, Neurotranscriptome profiles of multiple zebrafish strains. *Genomics Data* **5**, 206–209 (2015).
36. S. Okuyama, H. Marusawa, T. Matsumoto, Y. Ueda, Y. Matsumoto, Y. Endo, A. Takai, T. Chiba, Excessive activity of apolipoprotein B mRNA editing enzyme catalytic polypeptide 2 (APOBEC2) contributes to liver and lung tumorigenesis. *Int. J. Cancer.* **130**, 1294–1301 (2012).
37. H. Chen, S. A. Detmer, A. J. Ewald, E. E. Griffin, S. E. Fraser, D. C. Chan, Mitofusins Mfn1 and Mfn2 coordinately regulate mitochondrial fusion and are essential for embryonic development. *J. Cell Biol.* **160**, 189–200 (2003).
38. A. V. Anzalone, P. B. Randolph, J. R. Davis, A. A. Sousa, L. W. Koblan, J. M. Levy, P. J. Chen, C. Wilson, G. A. Newby, A. Raguram, D. R. Liu, Search-and-replace genome editing without double-strand breaks or donor DNA. *Nature* **576**, 149–157 (2019).
39. D. Tondera, S. Grandemange, A. Jourdain, M. Karbowski, Y. Mattenberger, S. Herzig, S. Da Cruz, P. Clerc, I. Raschke, C. Merkwirth, S. Ehses, F. Krause, D. C. Chan, C. Alexander, C. Bauer, R. Youle, T. Langer, J. C. Martinou, SLP-2 is required for stress-induced mitochondrial hyperfusion. *EMBO J.* **28**, 1589–1600 (2009).
40. N. Zemirli, M. Pourcelot, G. Ambroise, E. Hatchi, A. Vazquez, D. Arnoult, Mitochondrial hyperfusion promotes NF-κB activation via the mitochondrial E3 ligase MULAN. *FEBS J.* **281**, 3095–3112 (2014).
41. D. F. Suen, K. L. Norris, R. J. Youle, Mitochondrial dynamics and apoptosis. *Genes Dev.* **22**, 1577–1590 (2008).
42. M. Ott, J. D. Robertson, V. Gogvadze, B. Zhivotovsky, S. Orrenius, Cytochrome c release from mitochondria proceeds by a two-step process. *Proc. Natl. Acad. Sci. U. S. A.* **99**, 1259–1263 (2002).
43. H. Takuma, S. Kwak, T. Yoshizawa, I. Kanazawa, Reduction of GluR2 RNA editing, a molecular change that increases calcium influx through AMPA receptors, selective in the spinal ventral gray of patients with amyotrophic lateral sclerosis. *Ann. Neurol.* **46**, 806–815 (1999).
44. R. Raghava Kurup, E. K. Oakes, A. C. Manning, P. Mukherjee, P. Vadlamani, H. A. Hundley, RNA binding by ADAR3 inhibits adenosine-to-inosine editing and promotes expression of immune response protein MAVS. *J. Biol. Chem.* **298**, 102267 (2022).
45. B. E. Hjelm, B. Rollins, F. Mamdani, J. C. Lauterborn, G. Kirov, G. Lynch, C. M. Gall, A. Sequeira, M. P. Vawter, Evidence of mitochondrial dysfunction within the complex genetic etiology of Schizophrenia. *Mol. Neuropsychiatry* **1**, 201 (2015).
46. R. C. Roberts, Postmortem studies on mitochondria in schizophrenia. *Schizophr. Res.* **187**, 17 (2017).
47. S. Yamada, Y. Kubo, D. Yamazaki, Y. Sekino, Y. Kanda, Chlorpyrifos inhibits neural induction via Mfn1-mediated mitochondrial dysfunction in human induced pluripotent stem cells. *Sci. Rep.* **7**, 40925 (2017).
48. S. A. Detmer, D. C. Chan, Complementation between mouse Mfn1 and Mfn2 protects mitochondrial fusion defects caused by CMT2A disease mutations. *J. Cell Biol.* **176**, 405 (2007).
49. S. Sharma, J. Wang, E. Alqassim, S. Portwood, E. Cortes Gomez, O. Maguire, P. H. Basse, E. S. Wang, B. H. Segal, B. E. Baysal, Mitochondrial hypoxic stress induces widespread RNA editing by APOBEC3G in natural killer cells. *Genome Biol.* **20**, 1–17 (2019).
50. F. Burté, V. Carelli, P. F. Chinnery, P. Yu-Wai-Man, Disturbed mitochondrial dynamics and neurodegenerative disorders. *Nat. Rev. Neurol.* **11**, 11–24 (2014).
51. D. Kim, J. M. Paggi, C. Park, C. Bennett, S. L. Salzberg, Graph-based genome alignment and genotyping with HISAT2 and HISAT-genotype. *Nat. Biotechnol.* **37**, 907–915 (2019).

52. D. Smedley, S. Haider, S. Durinck, L. Pandini, P. Provero, J. Allen, O. Arnaiz, M. H. Awedh, R. Baldock, G. Barbiera, P. Bardou, T. Beck, A. Blake, M. Bonierbale, A. J. Brookes, G. Bucci, I. Buetti, S. Burge, C. Cabau, J. W. Carlson, C. Chelala, C. Chrysostomou, D. Cittaro, O. Collin, R. Cordova, R. J. Cutts, E. Dassi, A. Di Genova, A. Djari, A. Esposito, H. Estrella, E. Eyras, J. Fernandez-Banet, S. Forbes, R. C. Free, T. Fujisawa, E. Gadaleta, J. M. Garcia-Manteiga, D. Goodstein, K. Gray, J. A. Guerra-Assunção, B. Haggarty, D. J. Han, B. W. Han, T. Harris, J. Harshbarger, R. K. Hastings, R. D. Hayes, C. Hoede, S. Hu, Z. L. Hu, L. Hutchins, Z. Kan, H. Kawaji, A. Keliet, A. Kerhornou, S. Kim, R. Kinsella, C. Klopp, L. Kong, D. Lawson, D. Lazarevic, J. H. Lee, T. Letellier, C. Y. Li, P. Lio, C. J. Liu, J. Luo, A. Maass, J. Mariette, T. Maurel, S. Merella, A. M. Mohamed, F. Moreews, I. Nabihoudine, N. Ndegwa, C. Noirot, C. Perez-Llamas, M. Primig, A. Quattrone, H. Quesneville, D. Rambaldi, J. Reecy, M. Riba, S. Rosanoff, A. A. Saddiq, E. Salas, O. Sallou, R. Shepherd, R. Simon, L. Sperling, W. Spooner, D. M. Staines, D. Steinbach, K. Stone, E. Stupka, J. W. Teague, A. Z. D. Ullah, J. Wang, D. Ware, M. Wong-Erasmus, K. Youens-Clark, A. Zadissa, S. J. Zhang, A. Kasprzyk, The BioMart community portal: An innovative alternative to large, centralized data repositories. *Nucleic Acids Res.* **43**, W589–W598 (2015).
53. K. L. Howe, P. Achuthan, J. Allen, J. Allen, J. Alvarez-Jarreta, M. Ridwan Amode, I. M. Armean, A. G. Azov, R. Bennett, J. Bhai, K. Billis, S. Boddu, M. Charkhchi, C. Cummins, L. da Rin Fioretto, C. Davidson, K. Dodiya, B. El Houdaigui, R. Fatima, A. Gall, C. G. Giron, T. Grego, C. Guijarro-Clarke, L. Haggerty, A. Hemrom, T. Hourlier, O. G. Izuogu, T. Juettemann, V. Kaikala, M. Kay, I. Lavidas, T. Le, D. Lemos, J. G. Martinez, J. C. Marugán, T. Maurel, A. C. McMahon, S. Mohanan, B. Moore, M. Muffato, D. N. Oheh, D. Paraschas, A. Parker, A. Parton, I. Prosovetskaia, M. P. Sakthivel, A. I. Abdul Salam, B. M. Schmitt, H. Schuilenburg, D. Sheppard, E. Steed, M. Szpak, M. Szuba, K. Taylor, A. Thormann, G. Threadgold, B. Walts, A. Winterbottom, M. Chakiachvili, A. Chaubal, N. de Silva, B. Flint, A. Frankish, S. E. Hunt, G. R. Ilsley, N. Langridge, J. E. Loveland, F. J. Martin, J. M. Mudge, J. Morales, E. Perry, M. Ruffier, J. Tate, D. Thybert, S. J. Trevanion, F. Cunningham, A. D. Yates, D. R. Zerbino, P. Flicek, Ensembl 2021. *Nucleic Acids Res.* **49**, D884–D891 (2021).
54. K. Wang, M. Li, H. Hakonarson, ANNOVAR: Functional annotation of genetic variants from high-throughput sequencing data. *Nucleic Acids Res.* **38**, e164 (2010).
55. RepeatMasker Home Page;www.repeatmasker.org/.
56. CRAN - Package gplots;https://cran.r-project.org/web/packages/gplots/index.html).
57. S. Anders, P. T. Pyl, W. Huber, HTSeq—A Python framework to work with high-throughput sequencing data. *Bioinformatics* **31**, 166 (2015).
58. D. Kim, B. Langmead, S. L. Salzberg, HISAT: A fast spliced aligner with low memory requirements. *Nat. Methods* **12**, 357–360 (2015).
59. A. Zeisel, A. B. Muñoz-Manchado, S. Codeluppi, P. Lönnerberg, G. La Manno, A. Juréus, S. Marques, H. Munguba, L. He, C. Betsholtz, C. Rolny, G. Castelo-Branco, J. Hjerling-Leffler, S. Linnarsson, Cell types in the mouse cortex and hippocampus revealed by single-cell RNA-seq. *Science* **347**, 1138–1142 (2015).
60. W. Zhao, J. L. Pollack, D. P. Blagev, N. Zaitlen, M. T. McManus, D. J. Erle, Massively parallel functional annotation of 3′ untranslated regions. *Nat. Biotechnol.* **32**, 387–391 (2014).
61. M. G. Gordon, F. Inoue, B. Martin, M. Schubach, V. Agarwal, S. Whalen, S. Feng, J. Zhao, T. Ashuach, R. Ziffra, A. Kreimer, I. Georgakopoulous-Soares, N. Yosef, C. J. Ye, K. S. Pollard, J. Shendure, M. Kircher, N. Ahituv, lentiMPRA and MPRAflow for high-throughput functional characterization of gene regulatory elements. *Nat. Protoc.* **15**, 2387–2412 (2020).
62. T. Ashuach, D. S. Fischer, A. Kreimer, N. Ahituv, F. J. Theis, N. Yosef, MPRAnalyze: Statistical framework for massively parallel reporter assays. *Genome Biol.* **20**, 183 (2019).
63. J. T. Robinson, H. Thorvaldsdóttir, W. Winckler, M. Guttman, E. S. Lander, G. Getz, J. P. Mesirov, Integrative genomics viewer. *Nat. Biotechnol.* **29**, 24 (2011).

Acknowledgments: We thank D. Chan (California Institute of Technology) and O. Shirihai (UCLA) for sharing the Mfn1/2 knockout MEF and WT cells and the Mfn1 overexpression constructs. We thank J. Huang (UCLA) for sharing HEK293 cells. We appreciate the helpful discussions with C. Koehler and A. Van der Bliek. We thank N. Prunet and the MCDB/BSCRC Microscopy Core for training and microscope facilities. We thank members of the Xiao laboratory for helpful discussions and comments on this work. We thank the PsychENOCDE and COmmonMind consortia for making available the RNA-seq data used in this study. **Funding:** This work was supported in part by grants from the National Institutes of Health (R01MH123177 and R01AG075206 to X.X. and R01AG037514 and RF1AG049157 to D.W.W.). M.C. and T.W.C. were supported by the NIH T32LM012424. T.F. was supported by the UCLA Hyde Fellowship and Dissertation Year Fellowship. K.A. was supported by the University of California-Historically Black Colleges and Universities (HBCUs) Fellowship. **Author contributions:** Conceptualization: M.C., J.H.B., and X.X. Methodology: M.C., T.F., T.W.C., K.A., J.H.B., H.-I.J., and S.P. Investigation: M.C., T.F., T.W.C., K.A., J.H.B., H.-I.J., and S.P. Visualization: M.C. and J.H.B. Supervision: X.X., D.W.W., and J.H.B. Writing—original draft: M.C., T.F., T.W.C., K.A., J.H.B., and X.X. Writing—review and editing: M.C., T.F., T.W.C., K.A., J.H.B., H.-I.J., S.P., D.W.W., and X.X. **Competing interests:** The authors declare that they have no competing interests. **Data and materials availability:** All data needed to evaluate the conclusions in the paper are present in the paper and/or the Supplementary Materials. Postmortem brain RNA-seq data were obtained from Synapse.org [BrainGVEX (syn3270015), CMC (syn22344687), HBCC (syn32183303), and LIBD (syn22344123)].

Submitted 21 September 2022
Accepted 8 March 2023
Published 7 April 2023
10.1126/sciadv.ade9997